Wind Turbine Wakes - Control and Vortex Shedding

by

Davide Medici

March 2004
Technical Reports from
KTH Mechanics
Royal Institute of Technology
S-100 44 Stockholm, Sweden

Akademisk avhandling som med tillstånd av Kungliga Tekniska Högskolan i Stockholm framlägges till offentlig granskning för avläggande av teknologie licentiateexamen torsdagen den 25:e mars 2004 kl 10.30 i seminarierum 40, Teknikringen 8, KTH, Stockholm.

Universitetsservice US AB, Stockholm 2004

D. Medici 2004, **Wind Turbine Wakes - Control and Vortex Shedding**

KTH Mechanics, Royal Institute of Technology
S-100 44 Stockholm, Sweden

Abstract

Wind tunnel studies of the wake behind a model wind turbine have been made in order to get a better understanding of wake development as well as the possibility to predict the power output from downstream turbines working in the wake of an upstream one. Both two-component hot-wire anemometry as well as particle image velocimetry (PIV) have been used to map the flow field. All three velocity components were measured both for the turbine rotor normal to the oncoming flow as well as with the turbine inclined to the free stream direction (the yaw angle was varied from 0 to 30 degrees). The measurements showed, as expected, a wake rotation in the opposite direction to that of the turbine. A yawed turbine is found to clearly deflect the wake flow to the side showing the potential of controlling the wake position by yawing the turbine. The power output of a yawed turbine was found to vary nearly as the square of the cosine of the yaw angle. The possibility to use active wake control by yawing an upstream turbine was evaluated and was shown to have a potential to increase the power output significantly for certain configurations.

An unexpected feature of the flow was that spectra from the time signals showed the appearance of a low frequency fluctuation both in the wake and in the flow outside. This fluctuation was found both with and without free stream turbulence and also with a yawed turbine. The non-dimensional frequency (Strouhal number) was independent of the free-stream velocity and turbulence level but increases with the yaw angle. However the low frequency fluctuations were only observed when the tip speed ratio (or equivalently the drag coefficient) was high. This is in agreement with the idea that the turbine shed structures as a bluff body. It is hypothesized that the observed meandering of wakes in field measurements is due to this shedding.

Descriptors: Wind Energy, Power Optimisation, Active Control, Yaw, Vortex Shedding, Wake Meandering

Preface

The first part of this thesis consists of an introduction to wind energy, its potential and principles, a review of relevant work, a description of the techniques and equipment used in the experiments and a short summary of the results. The second part consists of three research papers which describe the results in detail. The contents of the papers have not been changed as compared to the published versions, except for some typographical errors, but they have been adapted to the present thesis format.

"*Like all other arts, the Science of Deduction and Analysis is one which can only be acquired by long and patient studies, nor is life long enough to allow any mortal to attain the highest possible perfection in it.*"

Holmes, S. (1887) A study in scarlet.

Contents

CHAPTER 1

Introduction

1.1. World energy resources and production

The growing demand of electricity in the world is stressing the traditional sources of energy. For instance, Europe is importing 50% of its energy needs, mainly in form of oil products. An urgent question is how this increased energy demand can be met in an environmentally friendly way. Can wind power provide one answer? The environmental factor is in favour of wind energy because wind is there to use and its use does not produce any green-house emissions.

The principle behind wind energy production is to convert the kinetic energy of the wind into a torque which turns the shaft of an electrical generator. Two limits are obvious: the first is when the turbine is leaving the wind speed unchanged, without extracting any energy. The second is when all the energy of the air that meets the turbine is extracted, however this is not possible since it would mean that the flow has stopped right behind the turbine. The optimal energy production occurs somewhere in between, and it is known as the Betz limit and will be discussed in chapter 2.

The total power in the wind, i.e. the kinetic energy per unit time in the stream tube approaching the wind turbine, is proportional to the cube of the wind speed. This means that the turbine should be elevated as far as possible from the ground, since the velocity in the atmospheric boundary layer decreases towards the ground. The energy extracted is also directly proportional to the diameter of the turbine itself. This factor makes it advantageous to make the turbine as large as possible and has resulted in the development of turbines of increasing size for large scale production.

1.1.1. *The potential of wind energy*

The *rated power* from a turbine (i.e. the maximum obtainable power) is only obtained if the wind speed is higher than a characteristic value, as shown in Fig. 1.1. A typical wind turbine runs below the rated power for approximately 75% of its production time. There is also an upper wind speed above which the turbine is shut down in order to avoid damages to the turbine.

The *installed capacity* of wind energy (for a wind turbine park, country or the world) is the sum of the rated power of all considered turbines. However, the energy produced during a certain time period can only be calculated if also

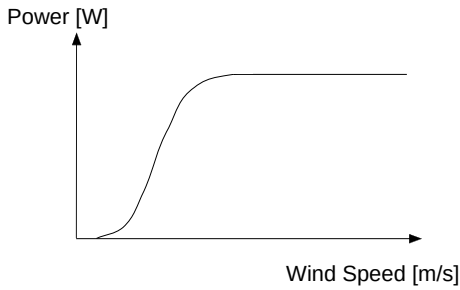

FIGURE 1.1. Power output as function of wind speed for a single wind turbine.

the velocity distribution in time is known for each turbine. Knowing the wind speed distribution, the energy output for a specific turbine can be calculated using a curve similar to Fig. 1.1.

Having the above analysis in mind, in order to understand if wind energy has a potential to develop even further, it is essential to understand the world wind resources. Data have been collected during many years in the 30 OECD (Organisation for Economic Co-operation and Development) countries, which includes Sweden since 1961, and in other areas of the world. The methodology, see for example Grubb & Meyer (1993), is to calculate the available land with an annual average wind speed higher than a chosen threshold value (in the cited case, above 5.1 m/s at a height of 10 m from the ground level). The energy output calculated from the velocity distribution is reduced by 90% when constraints such as high-populated areas, human activities, noise, visual impact, etc. are considered. An estimate of the available wind energy in TWh per year is shown in Fig. 1.3. This estimate refers to what wind turbines were able to produce one decade ago. Today's technology provides higher performances machines. The power of a wind turbine has raised from 0.4 MW at the above cited period to the modern 4 MW machines, manufactured by e.g. Enercon and General Electrics. One example of a modern wind turbine is the Enercon E66 which is shown in Fig. 1.2. It has a rated power of 2 MW and a diameter of 70 m.

Furthermore, no off-shore sites were considered by Grubb & Meyer (1993) whereas, today, great attention is focussed also on this area. For instance, the amount of energy which can be produced by off-shore sites in Europe is estimated in the order of 2000 TWh per year.

1.1.2. *Present world energy use*

When it comes to the statistics of the actual use of energy supplies, there exist small discrepancies between different studies due to differences in the definitions and methods used to evaluate the resources. Here the general definitions

FIGURE 1.2. Enercon E66. Courtesy of Enercon GmbH.

used by the International Energy Agency (IEA, www.iea.org) will be adopted. It states that *renewable energy sources* include hydro, geothermal, solar photovoltaics, solar thermal, tide, wave, ocean, wind, solid biomass, gases from biomass, liquid biofuels, and renewable municipal solid waste. For a more specific definition of each of the above mentioned sources, refer to the report by IEA (2002).

The produced energy in 2001 was $1.2 \cdot 10^5$ TWh[1]. If only electricity production is considered (about 15% of total production), renewables have provided 18% of the world total in 2001.

[1]This value is usually given in toe= tonne of oil equivalent and corresponds to 10038 Mtoe, 1 Mtoe = 11.63 TWh.

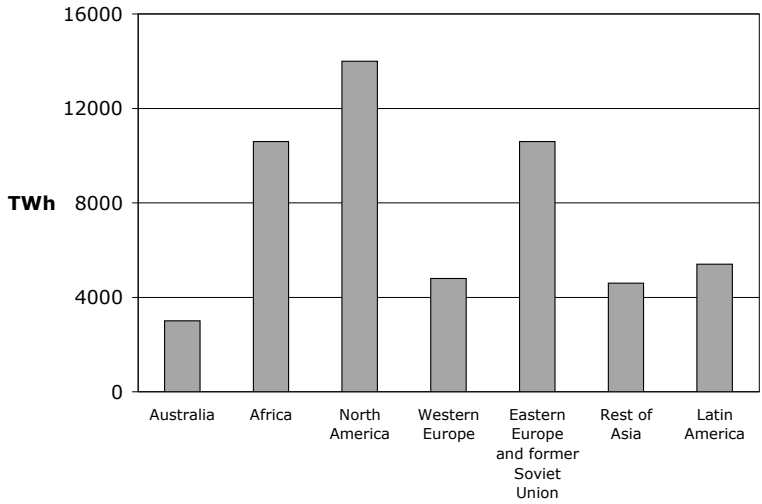

FIGURE 1.3. The world's wind resources, adopted from Grubb & Meyer (1993). The energy available from the wind is 53000 TWh per year.

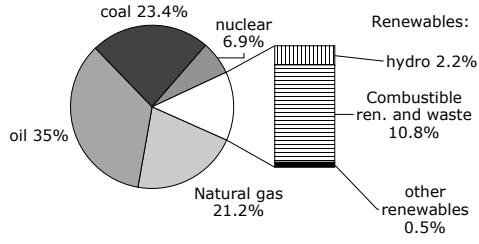

FIGURE 1.4. Fuel shares in world total primary energy supply for 2001 (IEA (2003)).

In the OECD countries, oil provided approximately 41% of the energy supply and renewable sources accounted for 5.7% of the total.[2] The division between the different renewable sources can be seen in Fig. 1.5. Once more, the situation differs for electricity production: renewable sources contributed with 1424 TWh of electricity in 2001, equal to 15% of the production. Wind

[2]The large value of 10.8% in Fig. 1.4 (as regarding the world total) for combustible renewables and waste stem from their heavy use in developing countries.

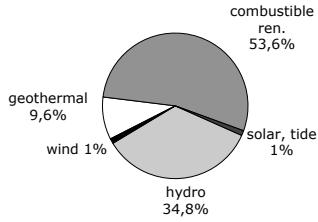

FIGURE 1.5. 2001 products' shares in OECD renewable energy supply, as from IEA (2003).

power contributed with 34 TWh, while hydropower was the main supplier of electricity with 13%. It is therefore clear that only a very small percentage of the wind energy potential is exploited (Fig. 1.3). The updated European situation of installed wind energy can be seen in Table 1.1. Other European countries accounted for 278 MW of installed capacity by June 2003.

Denmark is an interesting example of what can be achieved with wind energy. In Table 1.1, it is noticeable how the installed power capacity in 2003 was relatively small for this country, leader in the world of wind energy. A closer look to the data of Grubb & Meyer (1993) tells us that the theoretical energy production was estimated as 10 TWh. In 2001, Denmark produced

COUNTRY	Installed Jan-Jun 2003 [MW]	Total by June 2003 [MW]
Germany	835	12836
Spain	230	5060
Denmark	36	2916
Netherlands	125	803
Italy	12	800
UK	34	586
Sweden	36	364
Greece	57	354
France	72	220
Austria	80	219
Portugal	21	217
Ireland	0	137
Belgium	12	56
Finland	0	41
Luxembourg	0	16
Total	**1550**	**24626**

TABLE 1.1. European Union Capacity, June 2003. Source: www.ewea.org.

4.3 TWh of electricity by wind power. One may conclude that Denmark is levelling towards its maximum possible installed wind capacity. If so, it would be therefore a "reasonable" estimate to consider the world's energy capability of the order of 20000 TWh, i.e. half of what estimated by Grubb & Meyer (1993).

1.1.3. *Wind turbine parks*

There are several aspects of wind turbines that contribute to the success or are a source of problems for wind energy. One of those is the presence of a power grid able to sustain the loads produced. In order to optimise the resources, wind turbines are often placed in clusters, so called wind farms. The power produced by each wind turbine is usually collected to a common power line and then taken to the local grid. The final power line has to be able to handle the produced power, therefore very remote areas are often not convenient. In Denmark, where the electricity from wind power is approximately 18% of the country's need, the surplus of energy in the electrical grid has been found to be well managed also during very windy days by redirecting the loads on less used sections of the grid. This possibility plays an important role in Europe, since all grids are interconnected and the electricity can be easily directed somewhere else if not used where produced.

The transport of the wind turbine parts during the assembling process or in case of failure of a component should be as effective (and thereby inexpensive) as possible. Nowadays more and more wind farms are built off-shore. The distance from the coast is limited by the length of the power connection, the depth of the sea (typically a maximum of 30 m is chosen) and the accesibility of the site for maintenance operations. Off-shore, problems arise with the presence of less friendly conditions like waves, salt, ice and other seasonal weather conditions. On the other hand, the atmospheric boundary layer is more suitable for use at sea: lower turbulence, i.e. lower loads on the structures, and higher velocity at the same height compared with the boundary layer over the land. These factors entail the possibility for larger turbine diameters and lower towers than for wind turbines on-shore. The public perception is also more friendly since the turbines are further away.

Setting up a wind farm encounters many problems, only partially technical. Some of the logistic difficulties have been mentioned above. An estimate of the cost for installing an on-shore wind turbine is 900 EUR/kW rated power. Differences between on-shore and off-shore are evident in the division of the costs: on-shore 70% is accounted for the turbine itself, while off-shore the proportions are changed with a more costly foundation and an higher total cost, although these values strongly depend on the site. Thanks to the continuous progresses in wind power technology, e.g. the improvement in the design and the increase in size, the cost of the electricity in the last years has quickly fallen, as can be seen in Fig. 1.6. A projection for the short term is also included.

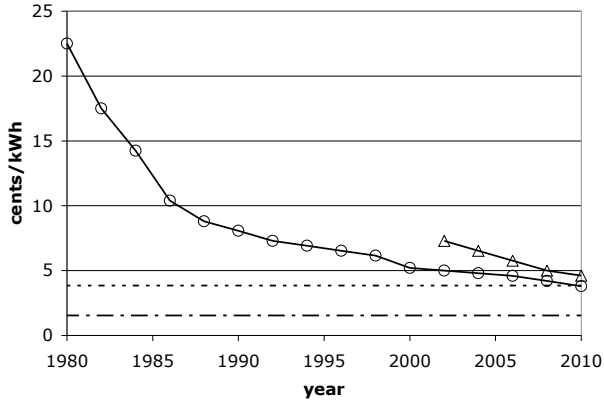

FIGURE 1.6. Production cost per kWh for the largest wind turbines on the market at a given time, from Jones (2003). ◯: on-shore installation, △: off-shore installation. The minimum and maximum market prices are indicatively represented with dashed lines.

1.2. Future development

In the previous sections the potential for wind power has been discussed: the resources are substantial and the technology is allowing their use in competition with other sources of energy. The political determination is crucial for the future. Several organisations are now regrouping in Europe under the *European Renewable Energy Council*. As a part of it, the European Wind Energy Agency not only monitors the development of wind energy, but sets targets for future developments. The predicted goals have always been exceeded by the achievements, as can be seen in Table 1.2.

In year 2000 wind energy contributed in Europe with 0.9% of the electricity production; now the target is to increase the production up to 12.9% by 2020, which will mean 444 TWh in that year (Table 1.2). To achieve this, two future scenarios have been proposed (Zervos (2003)). In the first the annual installation of wind power is assumed as increasing with a steady trend, although lower than what observed in the last five years. The target is set to 75 GW of installed capacity in Europe by 2010. A second more restrictive scenario assumes instead a decrease in the annual installations (compared to the last two years), and a levelling to 3800 MW per year of installed power. The target is set for this case to 60 GW by 2010. In any case wind energy will play a substantial role in the electric energy supply chain.

1.3. Objectives of the thesis

Wind turbines in a park are often placed in parallel lines, with the distance between the lines of the order of 5 to 9 diameters. The orientation is best

year	predicted [GW]	achieved [GW]
1991	4 in 2000	12.8
	100 in 2030	
1997	8 in 2000	12.8
	40 in 2010	
	100 in 2020	
2000	60 in 2010	
	incl. 5 offshore	
	150 in 2020	
	incl. 50 offshore	
2003	**75 in 2010**	
	incl. 10 offshore	
	180 in 2020	
	incl. 70 offshore	

TABLE 1.2. Wind energy capacity in Europe, EWEA targets. Zervos (2003).

when, for the prevailing wind direction, the interaction between the wake from an upstream wind turbine and a downstream one is minimised. The reason is not only that the power extracted is reduced by the velocity defect in the wake, but also the fatigue loads on the structures can become much higher. One objective of the thesis is to give a better understanding of the physical behaviour of turbine wakes by studying the wake behind rotating model turbines in a wind tunnel.

Another objective is to study the possibility of using the already existing yaw control on turbines in order to deflect the wake away from the downstream turbine. With this, loads on the shadowed turbine can be decreased and power production may be improved. The aim is to understand to what extent the side force created by the yawed turbine effects the wake and how the structure of the 3-dimensional wake is changed. An interesting observation is that the the turbine model sheds large scale structures in a similar way as a solid disc. These structures are assumed to be responsible for the meandering of the wake, which has been observed for example in field measurements in the Alsvik wind farm, on the island of Gotland. This kind of motion can be very important in wind parks, where interactions between several wakes can take place.

CHAPTER 2

Wind turbines: principles and design

2.1. Background

When the air flows around a streamlined body such as a wing profile, the pressure field is modified and therefore a force is generated. The component perpendicular to the flow direction is called *lift*, the component parallel to the inflow is the *drag*. The angle of attack between the blades and the direction of the relative wind is not only the result of the wind direction since the blade itself is moving. What happens can be clearly seen in Fig. 2.1 on one of the wind turbine models used for the experiments. The azimuthal velocity must be added to the wind speed, from left.

Some confusion as regarding the drag can arise. The force which is acting on the entire wind turbine in the same direction of the wind, is called drag as well. The application point of this force is the centre of the rotor, if the turbine is aligned with the uniform flow and the tower is neglected. Since the wind turbine studies are traditionally connected with the propeller area, this force is sometimes also called thrust.

For good performance of a wing, the separation of flow on the blade should be avoided. This is the reason why wind turbines have twisted blades: the

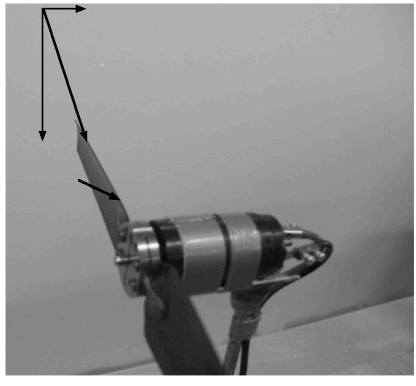

FIGURE 2.1. The angle between the plane of the rotor and the local wind direction is decreasing as moving towards the tip. The stall starts from the root.

angle of attack is optimised from tip to root, for the most frequent operational condition, by making the blade to turn out of the plane of rotation when moving towards the root. However the so-called *stall control*, one of the main aerodynamic controls on wind turbines, makes the stall to occur gradually from the root as the wind speed increases. The reason is to avoid high loads and also high power production which can cause problems to the electrical components of the wind turbine . This is a passive type of control, since the angle of attack on the blades increases with increasing wind speed.

A second important aerodynamic control present on wind turbines is the *yaw control*. It will be shown how the power is proportional to the cube of the wind speed normal to the rotor plane. To maximize the power output the wind turbine is turned towards the wind by means of electrical motors, which move the entire nacelle (i.e. the top part of the wind turbine including the shaft, the gearbox if present, the generator and the other systems) around the tower. Both the yaw control and the twist of the blades were well known in the past, when windmills produced not electrical but only mechanical energy. One example is the Morgan Lewis windmill, Barbados (Fig. 2.2) for which the pole connected to the backside of the "nacelle" was used to turn the blades towards the wind. The system required 10 men to be activated.

The third mostly used control is the *pitch control*. In this active control, the entire blade is turned, to optimise the angle of attack with respect to the wind. If the power output from the generator becomes too high, the system decreases the angle of attack of the blades, in order to obtain less power. This mechanism is the opposite of the *active stall control*, where the blades are instead turned out of the wind to increase the stall, thereby "wasting" the excess energy in the wind.

All the wind turbines have a cut-in wind speed, after which the wind generated torque is greater than the friction in the system and the rotor starts to rotate and produce electricity (see Fig. 1.1). The cut-off speed is instead the higher limit for the working conditions, above which the loads produced are considered dangerous for the machine. The range of velocities is typically somewhere between 3 m/s and 30 m/s, but depends on the type of wind turbine considered. When the conditions exceed the highest velocity limit, the turbine is stopped first by means of aerodynamic controls, e.g. pitching the blade and causing an extended stall, and then the brakes act on the shaft. Tip ailerons are also used in some models as aerodynamic breaks, or the entire tip itself is tilted.

Most wind turbines run at constant rotational speed, giving a constant frequency of the current produced. Small fluctuations in the frequency are allowed and adjusted with an electronic converter. The reason is that the turbines are connected to an electrical grid with a specific frequency of the current (50 Hz in Europe), which has to be matched by the production plant.

FIGURE 2.2. Morgan Lewis windmill, Barbados. The blades move a mechanism used to smash sugar canes. Built in 1727, it shows some technical solutions (yaw control and twisted blades) applied in order to improve its performance.

2.2. Theoretical estimate of power production

It is possible from so called actuator disc theory to establish an upper limit on the power production for a turbine. This is called the Betz limit and it is based on the mass and momentum conservation over a control volume which includes the turbine. Usually this is done by considering a stream tube as shown in Fig. 2.3, where the velocity is assumed to be uniform at each cross section of the tube. In a first approximation the wind turbine can be considered acting like a disc, the *actuator disc*, which has an infinite number of blades creating the needed pressure drop. The velocity along a streamline decreases when approaching the disc and therefore the atmospheric pressure p_∞ raises to the value p^+, according to Bernoulli to balance the velocity decrease. After the discontinuity surface of the actuator disc over which the pressure decreases, the pressure again increases from a lower value p^- to the initial, undisturbed value p_∞. The difference between p^+ and p^- gives the force acting on the disc.

The inflow and outflow boundaries are taken at such a distance that the pressure has recovered to the undisturbed atmospheric pressure (p_∞). The

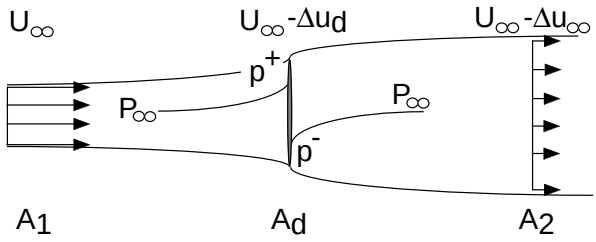

FIGURE 2.3. The wind speed is changed from upstream to downstream due to the presence of the actuator disc, which is represented in the middle of the graph.

power output of the turbine can be obtained in two different ways, either as the change of kinetic energy per unit time between the inflow and outflow boundaries, or as the force (pressure difference across the turbine times its area) times the velocity at the disc.

However, in the literature it is common that the momentum balance is taken over a stream tube of the form seen in Fig. 2.3, which in principle is not possible, since also the varying pressure (which is not equal to p_∞) on the mantle area of the stream tube has to be taken into account. It is possible to overcome this problem by considering a much larger stream tube which includes the one passing over the turbine. If the radius of that stream tube is large enough the pressure disturbance on the mantle surface will decay with the distance (r) from the turbine as r^{-2} and there will be no overall contribution from the pressure forces on the momentum balance. This means that the contribution of the pressure forces on the mantle surface in Fig. 2.3 actually equals $p_\infty \cdot (A_2 - A_1)$, cancelling exactly the pressure force due to the increase in the area at the downstream end of the stream tube.

In order to establish the Betz limit it is necessary to state the equations of conservation of mass and momentum. The mass flow ($\dot{m}$) which runs through the stream tube enclosing the turbine disc can be written

$$\dot{m} = \rho A_1 U_\infty = \rho A_2 U_2 = \rho A_d U_d \tag{2.1}$$

where A_1 and A_2 are the upstream and downstream areas of the stream tube and A_d is the actuator disc area. Using momentum conservation, the drag D on the turbine can, with the arguments used above, be written as

$$D = \dot{m} U_\infty - \dot{m} U_2 = \rho A_1 U_\infty^2 - \rho A_2 U_2^2 \tag{2.2}$$

By using Bernoulli's equation both upstream and downstream the turbine it is possible to obtain an expression for the pressure difference $p^+ - p^-$ across the turbine such that

$$p^+ - p^- = \frac{1}{2}\rho(U_\infty^2 - U_2^2) \tag{2.3}$$

and the drag on the turbine hence becomes

$$D = \frac{1}{2}\rho A_d(U_\infty^2 - U_2^2) = \rho A_d\left(U_\infty - \frac{\Delta u_\infty}{2}\right)\cdot \Delta u_\infty \tag{2.4}$$

where $U_2 = U_\infty - \Delta u_\infty$, i.e. Δu_∞ is the velocity defect in the wake at the downstream end of the stream tube. Using the same notation, Eq. 2.2 becomes

$$D = \dot{m}\left(U_\infty\right) - \dot{m}\left(U_\infty - \Delta u_\infty\right) = \dot{m}\Delta u_\infty = \rho A_d\left(U_\infty - \Delta u_d\right)\cdot \Delta u_\infty \tag{2.5}$$

where Δu_d is the velocity decrease at the turbine plane. A simple comparison between Eq. 2.4 and Eq. 2.5 gives the result known as Froude's theorem:

$$\Delta u_d = \frac{\Delta u_\infty}{2} \tag{2.6}$$

The total power in the wind, i.e. the kinetic energy passing a control area A per unit time, can be expressed as

$$P_{TOT} = \frac{1}{2}\rho A U_\infty^3 \tag{2.7}$$

The power extracted by the wind turbine on the other hand can be written as

$$P_E = \frac{1}{2}\dot{m}\left(U_\infty^2 - U_2^2\right) = \frac{1}{2}\dot{m}\left[U_\infty^2 - (U_\infty - \Delta u_\infty)^2\right] \tag{2.8}$$

which after some algebra can be rewritten

$$P_E = \rho A_d\left(U_\infty - \Delta u_d\right)^2\cdot 2\Delta u_d \tag{2.9}$$

The maximum power output is found by searching for the maximum in P_E with respect to the velocity defect at the disc Δu_d. From Eq. 2.9 we obtain

$$\frac{\partial P_E}{\partial \Delta u_d} = 0 \rightarrow \left(\Delta u_d\right)_{P_{Emax}} = \frac{U_\infty}{3} \tag{2.10}$$

The maximum power for the actuator disc with no losses, from Eq. 2.9 using Eq. 2.10, can be compared with the energy per time of the wind (Eq. 2.7) in order to obtain the efficiency of a turbine (Betz limit):

$$\frac{P_{Emax}}{P_{TOT}} = \frac{\frac{8}{27}\rho A_d U_\infty^3}{\frac{1}{2}\rho A_d U_\infty^3} = \frac{16}{27} \tag{2.11}$$

The drag and power are often expressed in terms of the non-dimensional drag coefficient C_D and the power coefficient C_P

$$C_D = \frac{D}{\frac{1}{2}\rho A_d U_\infty^2} \tag{2.12}$$

$$C_P = \frac{P}{\frac{1}{2}\rho A_d U_\infty^3} \tag{2.13}$$

In the Betz limit they become $\frac{8}{9}$ and $\frac{16}{27}$, respectively. For a real turbine both C_D and C_P varies with the tip speed ratio (λ), which is the ratio between the tip speed and the free stream velocity. We define it here as

$$\lambda = \frac{\Omega \cdot R}{U_\infty} \tag{2.14}$$

where Ω is the angular velocity of the turbine and R is the turbine radius.

2.3. Design

For modern wind turbines the rotor is often upwind with respect to the tower: loads on the blades created by the passage through the wake of the tower are avoided, as well as noise production. The blades are slightly tilted off the vertical plane, so that on the lower side the distance to the tower is increased to avoid a crash in case a strong wind bends the blades back. Two main concepts are presently on the market: the most common is connecting the shaft with an high speed generator through a gearbox which increases the rotational frequency, as in Fig. 2.4. Without the gearbox the stator is a large multi-layer ring, where the lower rotational frequency of the rotor is balanced by a greater number of poles in the stator. In this way the frequency of the produced current is increased and the machine can be directly connected to the electrical system.

For a given power output, the choice is then between a large, low speed rotor, or a smaller, high speed rotor, although hybrid system have been developed. Ultimately, both have some inconvenience. The weight of the nacelle is of the order of 3-400 tons for the gearless machine, and only about a fifth when the gearbox is present. Also the initial cost is generally in favour of a high speed generator, however the absence of moving parts is a pro-factor for the low speed generator. The gearbox has to stand the torque from the blades and the fluctuations of the wind speed and direction, which may cause it to break.

In the nacelle a small fixed crane can also be placed to considerably speed up the process of changing internal parts of the wind turbine. When it comes to assembling the machine, some interesting solutions can be seen. On-shore the process is usually easier: the machine is put together *in situ* connecting elements of the tower, of the nacelle and of the service parts (shaft, generator, active power controls, etc.). On the ground, in case of a three-bladed turbine, two blades are connected together and then lifted in front of the nacelle. At the end also the third blade is raised and bolted to the shaft.

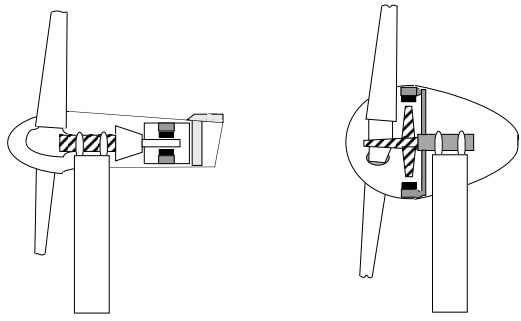

FIGURE 2.4. Figure showing the principles of a turbine with and without gearbox. Left: The gearbox is connecting the shaft, marked with the diagonal lines, and the high speed generator on the right side. At the far right a typical positioning of the cooling system. Right: Gearless machine. From left to right: the blades are connected to the rotor, the magnet (black) and the stator (grey) are visible.

Off-shore the environment is more challenging. First, the basement of the tower must be built. In a second stage, special-purpose ships with a crane are used and equipped with a number of poles which descend on the sea bottom and anchor the ship. On-shore the turbine is put together and then loaded on the ship, for example in only three pieces: the tower, the nacelle with two blades mounted, and a third single blade. The final assembling process of these parts can take place at sea in typical eight hours, if the weather conditions are good enough.

CHAPTER 3

Wind and wakes

In this chapter an introduction to the atmospheric boundary layer and a brief review on wind turbine wakes will be presented.

3.1. Atmospheric boundary layer

A wind farm operates within a region very close to the surface of the earth where the motion of air is strongly affected by a combination of pressure, frictional and Coriolis forces. In this region, called Atmospheric Boundary Layer (ABL), the velocity changes its value from zero at the ground to its full value in the outer part where frictional forces can be considered negligible.

Wind is created by differences in pressure in equal elevation points. These differences are mainly generated by temperature gradients (with associated variations in density) in the atmosphere. Normally neutrally stable boundary layers are considered, for which the influence of the temperature gradients can be neglected while the shear stresses are conditioned by the surface roughness. This assumption can be considered valid for relatively strong winds, which are interesting in the structural design of wind generators. Many reviews on the subject can be found in the literature. See for instance Monin (1970), Tennekes (1972) and Counihan (1975).

Following Monin (1970) it is possible to distinguish different layers within the ABL. The lowest part of the ABL close to the earth surface is called *surface layer*. In this layer the Coriolis forces can be considered negligible. The turbulence can be affected by density stratification which creates buoyancy forces. The effect of the density stratification in ABL decreases when approaching the surface. There is a sublayer, called the *dynamic sublayer*, in which this effect becomes negligible. It is well known that in a turbulent boundary layer on a smooth surface the Reynolds stresses are small compared to the viscous stresses and a viscous sublayer exists. However, land surfaces are always rough enough to force the boundary layer to be highly turbulent down to the surface, and no viscous sublayer can be generated.

Experimental analysis show that the structure of the ABL is very irregular. Such irregularities depend on different factors mainly linked to stratification, non-homogeneity of the temperature field and of course characteristics of the underlying surface. However, measurements show that an equilibrium state can be reached and the flow may become horizontally homogeneous if the wind

blows over an horizontal site of uniform roughness. The thickness can be kept constant due to the horizontal pressure gradient.

In the surface layer the mean velocity profile can be described by the following relation:

$$\frac{U}{U^*} = \frac{1}{\kappa} \ln\left(\frac{z-d}{z_0}\right) \tag{3.1}$$

where U is the mean velocity, U^* is the friction velocity, κ a constant, z the distance from the ground and d a displacement height that for flat surfaces can be set to zero. The term z_0 is a roughness parameter which strongly depends on the terrain considered. Generally very low values of this parameter as well as low turbulence intensities can be found off-shore. Eq. 3.1 is valid approximately till 10-15% of the boundary layer height.

In the upper part of the homogeneous ABL the mean velocity profile can be modelled by the following power law:

$$\frac{U}{U_{ref}} = \left(\frac{z}{z_{ref}}\right)^{\alpha} \tag{3.2}$$

where U_{ref} is the speed at the height z_{ref}, typically 10 m. It can be assumed that this law holds with a constant α up to the top of the boundary layer.

Counihan (1975) collected a large set of data describing the boundary layer parameters in a variety of situations. Turbulence values, power law indices and roughness parameters are listed by type (a city has a much different boundary layer than a rural area) and by site. A wind farm can be influenced by instabilities of the boundary layer, by a nearby forest or by the presence of a hill creating a separation region. The reader can refer to Monin (1970) or more recently to Wizelius (2002) for a more detailed discussion on the subject.

As far as the turbulence characteristics in the boundary layer the scenario is very complicated. In its large-scale limit the atmospheric turbulence approaches two-dimensionality, while its smaller scale forms are inherently three-dimensional. Normally, fluctuations of periods less than about one hour are considered as turbulence. Turbulence profiles are quite variable and depend on the terrain characteristics.

Important quantities in the ABL are the integral scales. They are basically a measure of the average size of the larger turbulent eddies associated with velocity fluctuations. Large eddies result in high correlations at large separations, which thus imply large integral scales. On the average the integral scales decrease with the height from the ground and with the increase of the terrain roughness. Some characteristics of the ABL for different categories of terrain are summarised in Table 3.1.

In wind tunnels there are two methods for the simulation of neutral atmospheric boundary layers. The first involves the use of long and rough surfaces, along which the boundary layer naturally grows. This method gives a good

Category	Type of terrain	z_0 [mm]	α	ABL height [m]
Smooth	ice, snow, sea	5-10	0.12	250
Moderately rough	open grassland	10-100	0.16	300
Rough	forests, suburbs	300-1000	0.28	400
Very rough	city centres	1000-5000	0.4	500

TABLE 3.1. Atmospheric boundary layer data, adopted from Counihan (1975).

representation of the real conditions, but requires very long test sections in order to have reasonable growth. Alternatively, a second method involves the use of artificial devices such as grids which are positioned inside the wind tunnel together with a rough surface accelerating the boundary layer growth (see for instance Talamelli *et al.* (2004)).

3.2. Wind turbine wakes

In this thesis the *wake* is defined as the region behind a wind turbine where the wind velocity has decreased as compared to its value far upstream the turbine. Wakes behind various types of bodies (two-dimensional, axis-symmetric and three-dimensional) have been extensively studied during the history of fluid mechanics. In principle a wake is generated by the loss of momentum due to the force on the fluid by the body (directed in the upstream direction). An equivalent force but with opposite sign is affecting the body itself and this force is usually called the drag force.

The flow characteristics and dimension of a wake depend to a large extent on the geometry of the body. For streamlined bodies the wake is small and of the order of the boundary layer thickness at the aft part of the body, whereas for bluff bodies the size of the wake region may be of the same order as the characteristic cross section dimension of the body. The flow field in the wake is usually highly complex, and depends both on the geometry of the body and the Reynolds number of the flow. For many cases vortical structures are present as a result of instability processes.

However, the wake development can for large downstream distances be described by self-similarity laws, which means that if appropriate variables are chosen, the mean profiles show similarity to each other independent of the downstream position. The self-similarity conditions may, however, depend on the geometry of the body. For instance, it has been shown by Bevilaqua & Lykoudis (1978) that the wake created by two bluff bodies of equal drag but different shapes does not reach the same self-similarity conditions. The reason is that, close to the sphere and the porous disc used in the experiments, different large vortex structures were generated.

As mentioned above instability processes may give rise to vortical structures in the wake. The most well known example is probably the Karman vortex street, which develops behind a circular cylinder if the Reynolds number is above 44. It has also been shown that the shedding frequency can be expressed as a non-dimensional frequency, the so called Strouhal number, which has been found to be constant over large Reynolds number ranges. Also three-dimensional bodies, such as a solid disc, may give rise to vortex shedding. Calvert (1967) showed that circular discs placed normal to the flow gave rise to a specific shedding frequency, however also inclined discs had similar shedding.

A wake behind a wind turbine model is even more complex than that behind a disc or cylinder, since in addition to the already mentioned flow phenomena the turbine sheds strong tip vortices as well as root vortices, giving a periodic upstream boundary condition for the wake. The vortices may also interact and pair with each other further downstream. Since a torque is produced by the turbine, this will also give rise to an overall rotation of the wake.

The wake from a turbine can be divided in two regions: the near wake and the far wake, Alfredsson *et al.* (1980) and Crespo *et al.* (1999). In the former region the wake centreline is constant as moving downstream until the shear layer (i.e. the region of velocity gradient) of the wake has reached the centreline because of turbulent diffusion, typically in 1 to 5 diameters, depending among other things on the ambient turbulence level.

For wind turbine wakes the region behind this initial development is usually called the far wake although self similar profiles are not reached until distances of the order of 30 diameters. As described in Crespo *et al.* (1999), the self-similarity is the basis for the kinetic modelling of wind turbine wakes. The review takes into account both single wake and wind farm modelling. A survey of the methods used to model wind turbine wakes can also be found in Leishman (2002). Experiments are often used to tune the modelling results.

In some cases discs have been used to simulate the wakes of wind turbines in wind tunnels, as e.g. in Sforza *et al.* (1981). The authors claim that matching the tip speed ratio of a wind turbine with a smaller model would change the flow-field characteristics because of the high rotational speed. Therefore these measurements focus on the drag coefficient. The same pressure drop as through a rotor is created by means of porous discs, which also avoid a large separation region. Several drag coefficients have been tested by changing the disc porosity. On the other hand a wind turbine has some characteristics which can be reproduced only by a rotating model, such as the tip vortices, the asymmetric induced velocity field in yawed conditions (e.g. as described in Schepers (1999)) as well as the overall wake rotation.

Experiments on rotating models are usually performed on one turbine or maximum two (Vermeulen (1980), Dahlberg & Medici (2003)) mainly because of the limited space in the wind tunnel. An exception to this is the simulation of a wind farm by Corten *et al.* (2003). They used 24 rotating turbine models, where the power output was measured and optimised

CHAPTER 4

Experimental Methods

4.1. Wind tunnels

4.1.1. *MTL wind tunnel (KTH)*

The Minimum Turbulence Level (MTL) wind tunnel at KTH Mechanics, was used in most of the experiments in this work. The tunnel (Fig. 4.1) is a closed-loop circuit, temperature controlled facility with a velocity speed up to 69 m/s. The test section is 7 m long, 1.2 m wide and 0.8 m high. The roof height of the test section can be adjusted in order to obtain a zero pressure gradient along the test section. The velocity variation achieved along the test section was less than 0.6% of the velocity measured by a Prandtl tube at 8 m/s. The Prandtl tube was placed for these experiments at approximately 1 m from the beginning of the test section, and provided the reference velocity for the calibration of the hot wire, as will be described in more detail later. A slot running along the test section length, in the middle of the roof, allows the access of the arm of the traversing system. With the addition of a wing spanning the full tunnel width, 5 degrees of freedom are possible. Added to the spatial x, y, z (i.e. respectively streamwise, vertical and spanwise) are the rotation around the probe axis and the rotation around the y-axis. A photograph of the test section can be seen in Fig. 4.2.

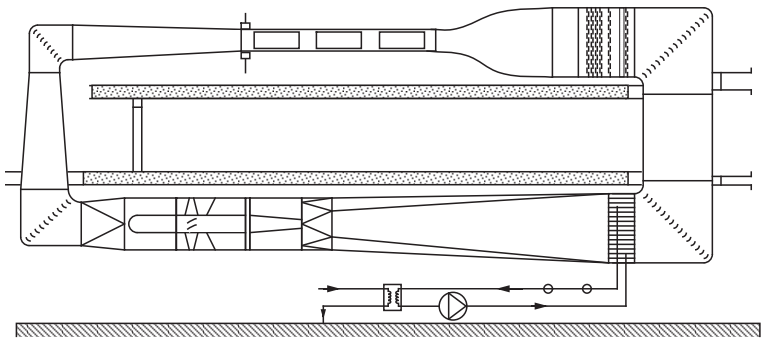

FIGURE 4.1. The MTL wind tunnel layout. The total length is about 25 m and the height is 9 m. The flow is anti-clockwise.

FIGURE 4.2. Test section with traversing system as seen from upstream.

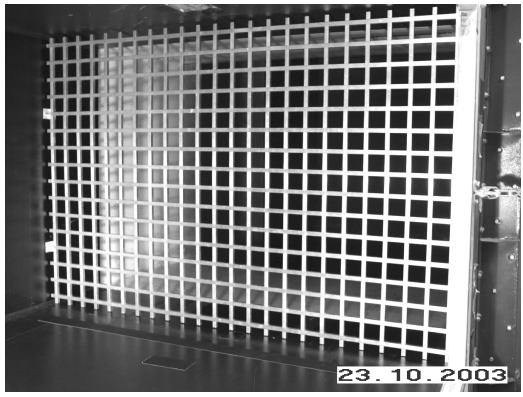

FIGURE 4.3. Turbulence generating grid used in the present experiments.

For some experiments free stream turbulence was generated by the grid shown in Fig. 4.3. The grid was fixed to the tunnel walls 0.2 m after the beginning of the test section, creating a turbulence intensity of approximately 4% of the free-stream velocity at the turbine position. The turbulence intensity for the three velocity components as percentage of the free-stream velocity is plotted in Fig. 4.4 as function of the downstream distance in mm. Without the grid generating the turbulence, the value of the fluctuations in the streamwise direction was less than 0.1% of the velocity measured by the Prandtl tube at 8 m/s.

A heat exchanger gives a very stable temperature control with an accuracy of ± 0.5 degrees by means of water cooling. The temperature is set manually

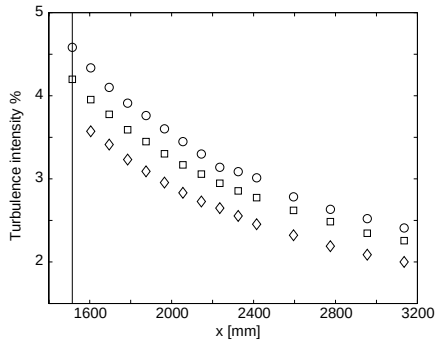

FIGURE 4.4. Turbulence intensity at the test section centre as function of downstream distance for the grid shown in Fig. 4.3. the grid is placed at x=200 mm and the vertical line in the figure represent the position of the turbine. ◯: u_{rms}, ◇: v_{rms}, □: w_{rms}.

at the control panel of the tunnel. Both the tunnel velocity and the traversing system are controlled by Labview programs. Also the data acquisition routines are Labview controlled. For more details about the MTL wind tunnel, the reader is referred to Lindgren (2002).

4.1.2. *LT-5 wind tunnel (FOI)*

The LT5 wind tunnel at FOI were mainly used for the drag interference measurements reported in **paper2**. Figure 4.5 shows the test section, the flow is from right to left. This open-loop wind tunnel has a test section 2.5 m long, with a cross section of 0.9m×0.675m. The velocity range is between 5 m/s and 16 m/s, and the tunnel is run by a centrifugal fan downstream of the test section. At the intake section, a grid helps to reduce the turbulence level. After a short contraction, the test section starts and the turbulence level is approximately 0.3% the free-stream velocity. The wind speed in the centre of the test section is found as the difference between the total pressure in the contraction and the static pressure given by four pressure taps, two upstream and two downstream the model position.

4.2. Measurement techniques

For the wake measurements, two techniques have been used: Particle Image Velocimetry (PIV) and hot-wire anemometry. In the described experiments, PIV gave an overall picture of the flow whereas the mean flow statistics were measured with hot-wire anemometry. Below follows a short description of the present set-ups for these two techniques.

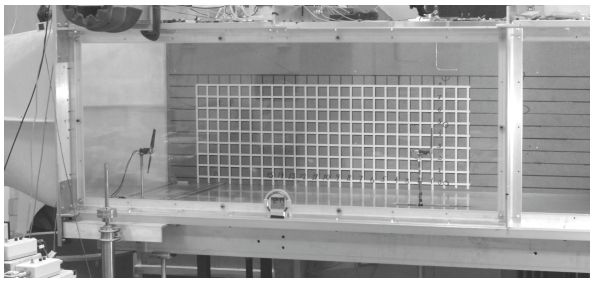

FIGURE 4.5. The test section of the LT5 wind tunnel at FOI.

4.2.1. *Particle Image Velocimetry*

The principle of PIV is simple: the speed of a particle is equal to the distance travelled during a certain time. If particles are added to the flow and they follow the flow, recordings of the particle paths allows us to study the velocity field.

In the present experiments the particle motions are recorded with a CCD camera where a laser sheet perpendicular to the camera lights the flow, i.e. the particles are imaged in one plane. The movements of the particles are registered between two times, t and $t + \Delta t$, where in the present case Δt is typically of the order of 100 μs. In this way the particles are allowed to move somewhere between 0.1 and 1 mm. The post-processing software divides the image in several rectangular regions, the so-called *interrogation areas*. In each of these areas the particle positions between the two recordings are correlated, resulting in the most probable displacement vector (Fig 4.6) during the time Δt.

Some of the factors which have to be set for each type of experiment are the choice of the particles and the time delay between the recordings. The particle size, the concentration in the fluid and body forces on the particles (if in very low speed flows) must also be considered in order for the particles to properly track the flow. In our experiment, propylene glycol oil with an average particle diameter of about 2 μm has been used to seed the flow, together with a 400 mJ Nd:YAG laser as the light source. The time between the two recordings has to be short enough so that only few particles exit the interrogation area. Such a particle has an effect on the signal-to-noise ratio, since its "true" correlated position is not detected. A reliable cross-correlation requires a minimum of 5 particles per interrogation area, and the size of the particles should be at least three pixels on the image in order to pick its correct position. As a rule of thumb the estimated displacement of a particle should not exceed 30% of the side length of the interrogation area. Measuring in regions with large velocity gradients can be a source of problems, since the output vector is an average over the interrogation area (therefore the gradient may be somehow smeared)

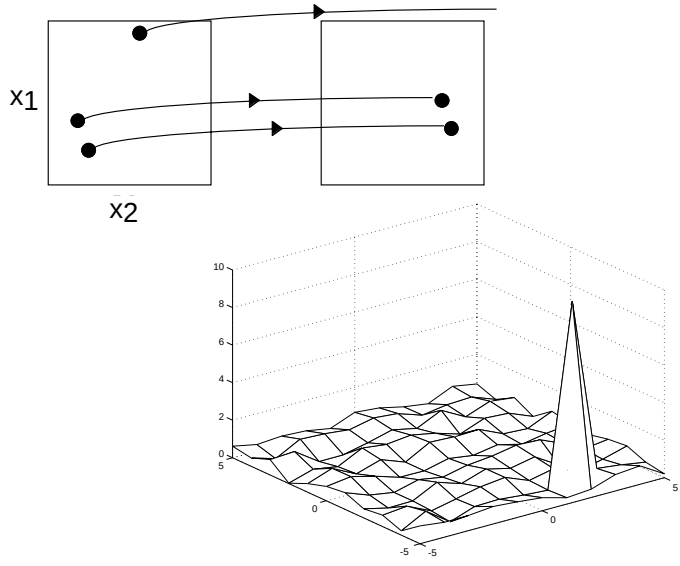

FIGURE 4.6. The correlation principle used in PIV. The sequel of two images from the CCD camera gives the most probable displacement vector in each interrogation area.

and the time chosen for the capturing should be different for different regions of the layer.

The acquisition frequency is mainly imposed by the frequency of the laser. In the experiment here discussed, this value is 14 Hz, which is also the frequency between each pair of images. The CCD camera has 1018×1008 pixels, and was divided in interrogation areas with 64×64 pixels. The side of each interrogation area is 2.7 mm, which is therefore the spatial resolution achieved with the PIV.

4.2.2. *Hot-wire anemometry*

Hot-wire anemometry is a technique where a thin wire (e.g. 5 μm in diameter and 1 mm long) of platinum is heated up to 100-200 degrees above the ambient temperarure. In Constant Temperature Anemometry (CTA) the wire is the fourth arm of a Wheatstone bridge. Depending on the local speed experienced by the wire, its resistance changes, and so does the voltage needed to balance the bridge. The voltage is a function of the velocity value, and the law describing this relation for one-component velocity measurements is known as the *modified King's Law*, see Johansson & Alfredsson (1982):

$$U = k_1(E^2 - E_0^2)^{\frac{1}{n}} + k_2\sqrt{E - E_0} \tag{4.1}$$

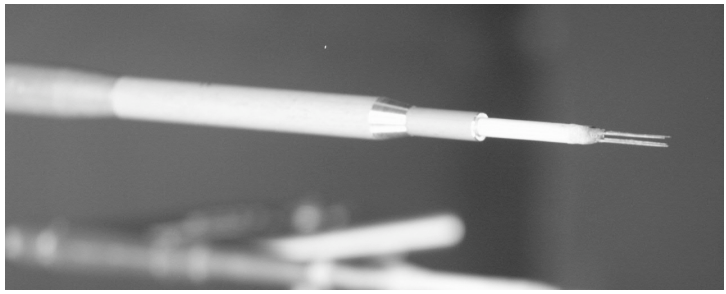

FIGURE 4.7. One of the X-wire used in the experiments. The flow is from right and the measuring volume is a cube with a side length of 1 mm.

where E is the measured voltage, E_0 the voltage at zero velocity, and k_1, k_2, n are the coefficients from the calibration. The wire is soldered to two prongs which are shaped in order to reduce their influence on the flow.

Using two wires placed approximately 45 degrees with respect to the flow direction, the two velocity components can be calculated as combination of the voltages output from the wires. In the calibration, the probe is turned to a known angle (from –40° to +40°) with respect to the free-stream velocity (from 1 m/s to 18 m/s) measured by a Prandtl tube. Two 2-dimensional fifth order polynomials are fitted to the voltages and the coefficients are calculated with the least square method. A typical calibration map is shown in Fig. 4.8.

Calibration points were taken down to a free stream velocity of 1 m/s. If lower velocities need to be measured by the hot-wire, this is not a problem when the modified King's law is used. The polynomials must instead include the velocity range of the measurements. The reason is that the fitting polynomials are not reliable outside the calibration range, since they can diverge to infinity. A solution was found in order to include also the points in the wake, e.g. close to the hub, where the velocity was lower than the allowed minimum of 1 m/s. The voltages from each wire, having in common the same angle with respect to the wind direction, were fitted to the modified King's law. In this way, the voltage values for lower velocities (namely 0.2 m/s and 0.5 m/s) were extrapolated and inserted in the calibration map of the X-wire. Differences were noticeable with the calibration corrected in this way.

4.3. Turbine models

The main advantage of doing simulation of wind turbines in a wind tunnel, as compared to the field measurements, is the controlled flow conditions. On the other hand, the Reynolds number can not be matched: the difference in chord is evident and wind speed must be kept low to avoid too high rotational speed. The latter may be a source of problem, since the centrifugal forces can modify

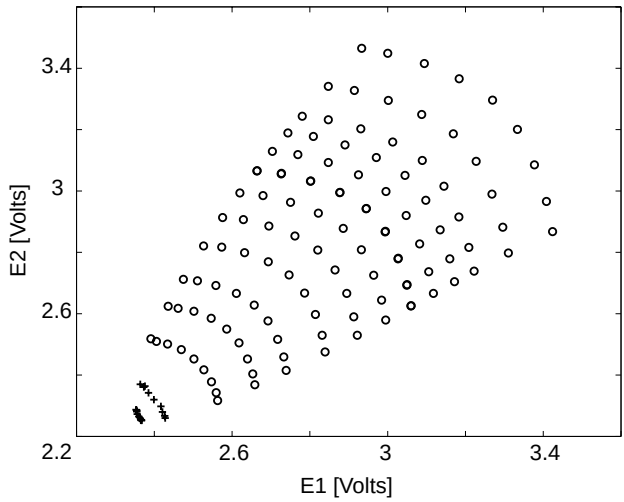

FIGURE 4.8. X-wire calibration map, where the two wires voltages are shown on the abscissa and ordinate, respectively. The circles represent calibration points from 1 m/s to 18 m/s and in 10° intervals with ±40°. The crosses are the values extrapolated using the modified King's law at 0.2 m/s and 0.5 m/s.

the boundary layer on the blades and the development of the wake itself. On the other hand, as mentioned by Vermeer *et al.* (2003), measurements at low Reynolds number are suitable for comparison with numerical models as long as an appropriate wing profile is chosen.

The power output of the turbine can simply be measured from the current and voltage across the generator. However in this case the internal friction as well as losses in the generator are not taken into account. By instead calibrating the generator to obtain the torque from the current its is possible to get the aerodynamic power efficiency.

The drag force measurements were carried out using a strain-gauge balance in the support of the model. When a load is applied, the deformation changes the resistance of the strange gauge. The calibration was made by fixing a known weight acting along the shaft of the generator, where also the rotor acts. The calibration curve can be seen in Fig. 4.9. The weights were measured by a precision balance, with an accuracy of the order of a milligram. The calibration shows a linear relation between the load and the electrical output from the balance.

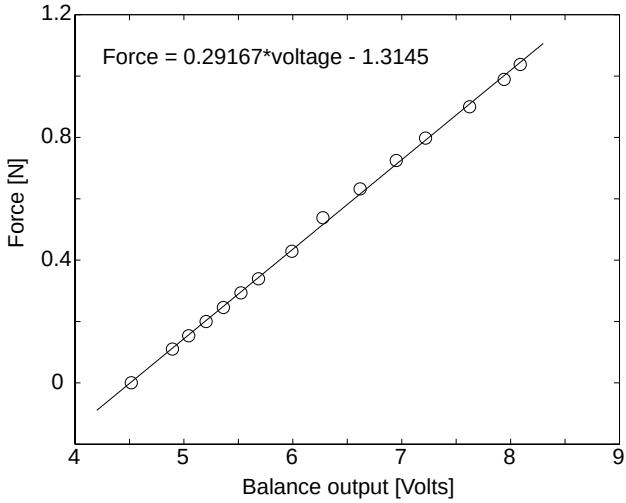

FIGURE 4.9. Drag balance calibration curve with calibration points.

r/R	Chord [mm]	Twist [deg]
0.25	32	15
0.50	35	11
0.75	31	5
1	25	3

TABLE 4.1. Turbine model 1 characteristics.

4.3.1. *Turbine model 1*

The turbine model 1 is used in paper 1. Its diameter is 0.25 m, it has two blades and high solidity (14%). The characteristics of the turbine are shown in Table 4.1.

The nacelle accommodates a generator and the turbine was controlled by a load circuit. This system enabled the change of the rotational frequency keeping the free-stream velocity constant. In this case the power output was calculated as product of the voltage and the current from the generator. The rotational frequency was measured using an optical device fixed under the nacelle, giving an electrical impulse at each blade passage. The turbine was tested at different heights from the floor: 0.248 m, 0.305 m and 0.4 m. No differences were

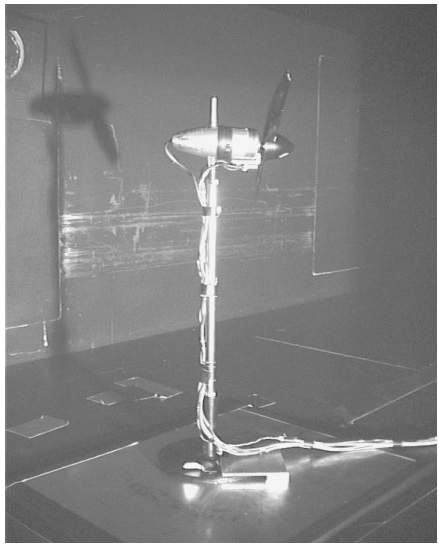

FIGURE 4.10. Turbine Model 1

noticed between these cases, so the chosen height was that with the turbine in the middle of the test section.

The turbine model is shown in Fig. 4.10. When rotating the turbine in yaw, the centre of rotation is directly below the hub of the turbine. The power coefficient for this turbine is shown in Fig. 4.11. The turbine tip speed ratio during the experiments was set such that the turbine operated close to its maximum power coefficient.

When the loading circuit is open, the turbine is free-running: no current flows through the circuit (i.e. no power is produced), and the torque has only to overcome the internal friction of the rotating parts. Therefore the rotational speed is at the maximum value, if the wind speed is kept constant. The open circuit can be achieved by also increasing the variable resistance to a value where the generator is unable to produce a current through the circuit. The opposite situation is when the resistance is zero, or the circuit is short-circuit.

4.3.1.1. *Yaw dependence*

Another characteristic investigated for this wind turbine is the variation of the power with the respect to the flow angle. In Fig. 4.12 the variation both of C_p and the tip speed ratio is shown for turbine model 1. Both the power curve and the tip speed ratio as function of the yaw angle showed a symmetric behaviour after a small offset was applied. The –1.8 degrees offset may be due to an a-symmetry in the turbine behaviour because of the direction of rotation. For this model the variation is nearly proportional to the square of $\cos\gamma$, whereas

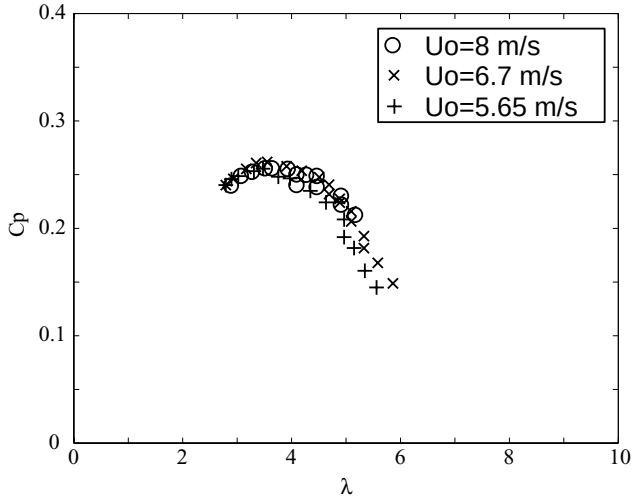

FIGURE 4.11. The power coefficient (C_p) versus tip speed ratio (λ) for three different free stream velocities.

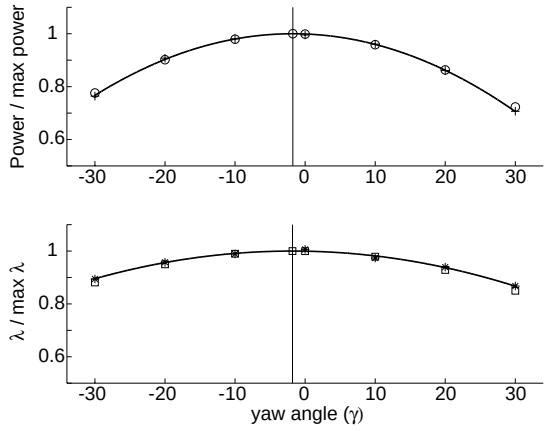

FIGURE 4.12. Power output and tip speed ratio (λ) vs. yaw angle at U_∞=6.3 m/s. The measurement points (+) are normalised with the maximum value obtained from each fitting curve. The squares denotes $\cos\gamma$, the circles denotes $\cos^2\gamma$.

the tip speed ratio varies linearly with $\cos\gamma$ when the loading on the turbine was constant.

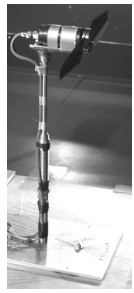

FIGURE 4.13. Turbine model 2.

4.3.2. *Turbine model 2*

A second turbine, built at FOI, was used in other sets of measurements in **paper 2** and **paper 3**. Its diameter is 0.18 m, and as the previous one it is two-bladed. For this turbine the blades are straight (i.e. no twist) and they are built out of four layers of carbon fibres giving a final thickness of 0.5 mm. The profile is based on the Göttingen 417A airfoil, chosen for its good performance at low Reynolds number. The chord at the tip is 16 mm and the maximum chord is 27 mm, at 12% of the radius. The solidity is 13%. The blades are attached by a screw, 3 mm in diameter, to the 23 mm nacelle. These screws allow the setting of the pitch angle of the blades, defined as the line connecting the leading edge to the trailing edge at 85% of the radius. A designated set-up was built at FOI to fix the pitch angle (see Montgomerie & Dahlberg (2003)) and allows an accuracy of ± 0.05 degrees.

The blade pair is connected to a 24V DC motor which works as a generator. In this case the torque was calibrated versus the output voltage and was shown to be a straight line. Hence the aerodynamic power produced by the turbine can be calculated.

The other important characteristic for a wind turbine is the drag[1] coefficient. The results in **paper 2** and **paper 3** show how the drag coefficient first increases with the tip speed ratio and then tends to level out at a value which is of the order of 0.9. During the experiments, the running conditions for the turbine, such as power and drag coefficients, were measured and compared before and after. No change has ever been observed, proving that the model had stable characteristics during the maximum 30 hours measurements period.

[1] As already mentioned the drag of the turbine is sometimes denoted as thrust.

CHAPTER 5

Summary of papers and authors contributions

The thesis is based on the following three papers.

Paper 1
Parkin, P., Holm, R. and Medici, D. "The application of PIV to the wake of a wind turbine in yaw", Proc. 4th International Symposium on Particle Image Velocimetry, Göttingen, 2001.

The experiment was led by PP and RH. The data processing and analysis was done by DM supervised by PP. The paper was written by PP and RH, whereas DM prepared the figures.

Paper 2
Dahlberg, J.–Å. and Medici, D. "Potential Improvement of wind turbine array efficiency by active wake control (AWC)", Proc. European Wind Energy Conference, Madrid, 2003.

The work was equally divided between the authors. The original idea of AWC was by JÅD.

Paper 3
Medici, D. and Alfredsson, P.H. "Measurements on a wind turbine wake: 3D effects and bluff-body vortex shedding".

The measurements were performed by DM, as well as the data analysis. The paper was written together with HAL.

5.1. Summary of papers

In **paper 1** the near wake downstream a rotating wind turbine model is studied using PIV, both with the turbine normal to the free stream direction and under yawed conditions. It is shown that yawing the turbine makes the wake deflect towards the side of the downstream blade, in response to a force perpendicular to the wind direction. The PIV used in the experiment allowed several instant pictures of the flow, and in specific of the tip vortices. The vortices, together with the rotation of the wake, seem to make the difference with the wake from another bluff body, as if the wake can be frozen until these vortices are

particularly strong and easily detectable. The effect of yawing can be seen in the mean velocity values, which are known every few millimetres thanks to the technique used for the measurements. The velocity in a chosen point can even double when the wake moves away.

In **paper 2** various effects on a single turbine under yaw is studied as well as the interaction between two turbines by traversing one turbine in the spanwise direction downstream an undisturbed turbine. In this way a direct measure of the power interference can be obtained, showing itself in terms of "power wakes". The effect of yaw on the power deficit is studied and a model for wind farm is used to predict the effect of active yaw control. It is shown that for a six turbine station an increase in power of about 4% can be achieved.

In **paper 3** the wind turbine wake is studied in more detail using two component hot-wire measurements. It is shown that the wake from a single wind turbine exhibits a large degree of non-symmetry respect to the central axis when yawed. The effect of free stream turbulence is also studied. An unexpected and interesting phenomenon was observed during the measurements, namely a large scale motion of the wake which reflects itself in low frequency variations as detected by the hot wire. The frequency, if expressed as a Strouhal number, is similar to what one would expect for shedding behind a solid disc and it was concluded that the turbine sheds vortices in a similar way as a disc. It was hypothesized that the meandering of the wake observed behind full scale turbines is due to such vortex shedding.

Acknowledgements

I want to thank first my supervisor Prof. Henrik Alfredsson for his guidance and advice which started during my master thesis period at the Lab. Enjoying Science is also experiencing knowledge through someone else (and trying to get as much as possible from it).

Special thanks go to Prof. Alessandro Talamelli for his advise and comments on the thesis.

A very special thanks goes to Jan-Åke Dahlberg. It has been a pleasure to work with a scientist and a friend. I hope to keep the same fun and joy in experiments as you are always able to communicate me. Sven-Erik Thor, Björn Montgomerie and all the FOI wind energy group are also acknowledged for many fruitful discussions and help.

Many special persons in the Lab made my staying here unique: Marcus and Ulf always have the perfect answer (and experimental set-ups) for every question. Dr. Nils Tillmark is acknowledged for his assistance and for his efforts in guiding the Ph-D students crowd toward a well-organised lab. Dr. Fredrik Lundell is the first person I met in Sweden and has been since then a constant reference for advice, friendship and discussions. Dr. Luca Brandt is the second person I met in Sweden and he has been always there for me. Don't ask me who was the third person I met, I can not remember. Many other people need to be mentioned: Jun, Luca F., Jens and everybody in the Lab and at the Department.

Thanks to my brother Dario, to Cesare, Luca S., Guido and to the volleyball team. My life would not be the same without all of you. Someone made a difference: I learned a lot and I will never forget.

Il mio lavoro sarebbe sicuramente diverso senza l'aiuto e l'appoggio che vengono dalla mia famiglia. Posso andare ovunque ma so che un riferimento e' sempre fermo ad aspettarmi. Grazie.

Bibliography

Alfredsson, P. H., Dahlberg, J. Å. & Bark, F. H. 1980 Some properties of the wake behind horizontal axis wind turbines. In *Proc. Third Int. Symp. on Wind Energy Systems*, Copenhagen, BHRA Fluid Engineering, paper J5, pp. 469–484.

Bevilaqua, P. M. & Lykoudis, P. S. 1978 Turbulence memory in self-preserving wakes. *J. Fluid Mech.* **89**, 589–606.

Calvert, J. R. 1967 Experiments on the flow past an inclined disk. *J. Fluid Mech.* **29**, 691–703.

Corten, G. P., Schaak, P. & Eecen, P. 2003 Heat and flux. In *Proc. European Wind Energy Conference and Exhibition*, Madrid, (published on CD).

Counihan, J. 1975 Adiabatic atmospheric boundary layers: a review and analysis of data from the period 1880-1972. *Atmos. Environ.* **9**, 871–905.

Crespo, A., Hernánedez, J. & Frandsen, S. 1999 Survey of modelling methods for wind turbine wakes and wind farms. *Wind Energy* **2**, 1–24.

Dahlberg, J. Å. & Medici, D. 2003 Potential improvement of wind turbine array efficiency by active wake control (AWC). In *Proc. European Wind Energy Conference and Exhibition*, Madrid, (published on CD).

Grubb, M. J. & Meyer, N. I. 1993 *Renewable Energy Sources for fuels and electricity*. Island Press, Washington DC.

IEA 2002 Renewables in global energy supplies, an IEA fact sheet. Technical Report, IEA statistics.

IEA 2003 Renewables information. Technical Report, IEA statistics.

Johansson, A. V. & Alfredsson, P. H. 1982 On the structure of turbulent channel flow. *J. Fluid Mech.* **122**, 295–314.

Jones, D. 2003 Will wind be the energy for tomorrow's generation? In *Proc. European Wind Energy Conference and Exhibition*, Madrid, (published on CD).

Leishman, J. G. 2002 Challenges in modelling the unsteady aerodynamics of wind turbines. *Wind Energy* **5**, 85–132.

Lindgren, B. 2002 Flow facility design and experimental studies of wall-bounded turbulent shear-flows. PhD thesis, TRITA-MEK Tech. Rep. 2002:16, Dept. Mech., KTH, Stockholm, Sweden.

Monin, A. S. 1970 The atmospheric boundary layer. *Annu. Rev. Fluid Mech.* **2**, 225–250.

Montgomerie, B. & Dahlberg, J. Å. 2003 Vortex system studies on small wind turbines. FOI scientific report, ISRN FOI-R–0936–SE.

Schepers, J. G. 1999 An engineering model for yawed conditions, developed on the basis of wind tunnel measurements. AIAA paper 99-0039, 18th ASME Wind Energy Symp., and 37th AIAA, Aerospace Sciences Meeting and Exhibit, Reno, also published in *Collection of Technical papers* (A99-17151 03-44).

Sforza, P. M., Sheerin, P. & Smorto, M. 1981 Three-dimensional wakes of simulated wind turbines. *AIAA J.* **19**, 1101–1107.

Talamelli, A., Riparbelli, L. & Westin, J. 2004 An active grid for the simulation of atmospheric boundary layers in wind tunnel. *Wind and Structures* **7**, in press.

Tennekes, H. 1972 The logarithmic wind profile. *J. Atmos. Sci.* **30**, 234–239.

Vermeer, L. J., Sørensen, J. N. & Crespo, A. 2003 Wind turbine wake aerodynamics. *Prog. Aerospace Sci.* **39**, 467–510.

Vermeulen, P. E. J. 1980 An experimental analysis of wind turbine wakes. In *Proc. Third Int. Symp. on Wind Energy Systems*, Copenhagen, BHRA Fluid Engineering, paper J3, pp.431–450.

Wizelius, T. 2002 *Vindkraft i teori och praktik*. Studentlitteratur.

Zervos, A. 2003 The future of wind energy in Europe. In *Proc. European Wind Energy Conference and Exhibition*, Madrid, (published on CD).

1

Paper 1

The application of PIV to the wake of a wind turbine in yaw

By P. Parkin, R. Holm and D. Medici

KTH Mechanics, SE-100 44 Stockholm, Sweden

Proc. 4th International Symposium on Particle Image Velocimetry, Göttingen, 2001.

PIV has been used in a wind tunnel study of the wake of a 0.25 m diameter two bladed model horizontal axis wind turbine (HAWT). Velocity fields of the wake from one to five rotor diameters downstream of the wind turbine model are shown, both with the turbine aligned in the flow and yawed. Data analysis is mainly based on time averaged velocity profiles of the wake for a range of yaw angles [0°, ±10°, ±20°, ±30°] in a plane parallel to the flow. Results show the size and persistence of the velocity deficit and tip vortices in the wake, and the wake deflection in yaw. It is shown that active control of turbine yaw angles could be an advantage for overall maximization of power output from wind farms.

---

1. Introduction

Wind power is now an established alternative to more conventional electrical power generation. To economise the utilisation of wind power, it is usual to group several units together in parks. Design criteria have to be developed for the interspacing of turbines to minimise interference between nearby turbines. Thus an understanding of wind turbine wakes is important. Even with careful placement of wind turbines within a wind park some interference, particularly at non-predominant wind directions, is inevitable. When a wind turbine is yawed the wake is deflected. Therefore, with the further understanding of wind turbines wakes in yaw, there is the possibility of actively controlling the yaw angle of an upstream turbine to steer the wake away from downstream turbines, thereby maximising the power output from the wind farm as a whole.

Wind turbines extract energy from the wind, therefore there is a consequential momentum loss downstream. In addition, previous gross wake investigations (e.g. Pedersen & Antoniou (1989)) have shown the wake to be dominated by tip vortices trailing from the blades, which later break down creating turbulence. Several aspects determine the wake development, such as the turbine operating conditions, the turbulence level in the flow field, the boundary layer shear and the distance to the ground plane. Hot-wire experiments by Alfredsson & Dahlberg (1979) investigated the velocity deficit in the wake from

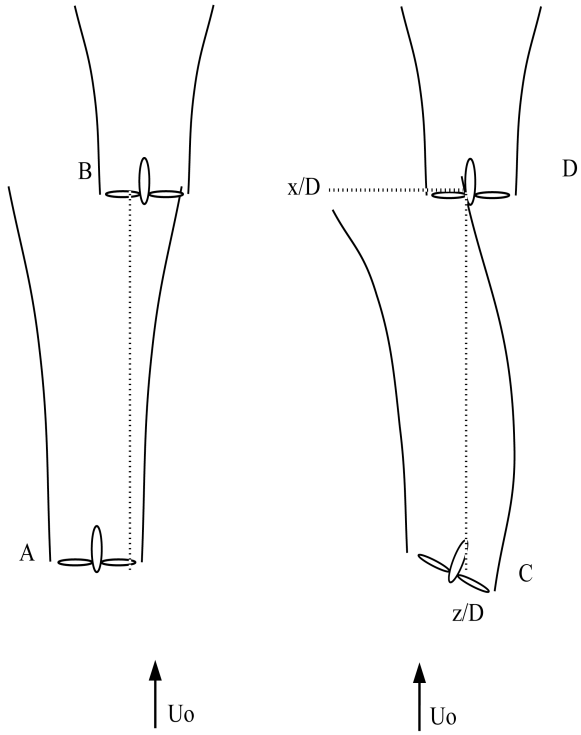

FIGURE 1. Turbine B is heavily disturbed by an unyawed turbine A. On the other hand, by yawing turbine C turbine D can work under much more favorable conditions compared to turbine B.

two to six diameters downstream in different free stream turbulence intensities, whilst Alfredsson & Dahlberg (1981) made interference measurements with two and three turbines in a wind tunnel. These and studies by Vermeulen (1980), Sforza *et al.* (1981), Ross & Milborrow (1985) and Smith & Taylor (1991) enabled simple interspacing models for wind farms to be formed. No experiments were performed with turbines operating in yaw, however.

The gross wake deflection in yaw was shown by Clayton & Filby (1982), who performed hot-wire measurements in the wake of a wind turbine at a number of downstream positions. PIV measurements in the near wake (up to one diameter downstream) by Grant *et al.* (1997) and Grant & Parkin (2000) have enabled a detailed understanding of vortex formation and expansion both in yawed and unyawed conditions, as well as the initial skew angle of the wake of a yawed turbine. This kind of detail in the very near wake is important for wake-vortex theories for performance predictions, but is less relevant when

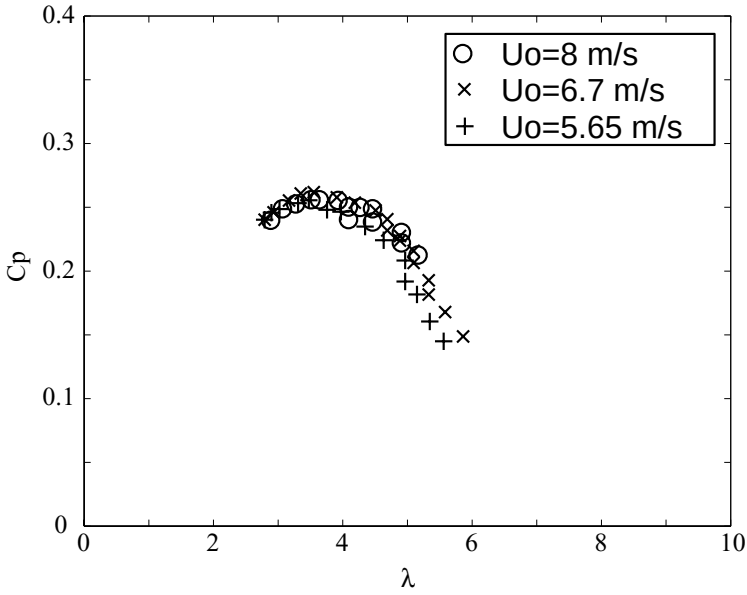

FIGURE 2. Power coefficient vs. tip speed ratio (λ) for different free-stream velocities for the model wind turbine. The collapsing of the curves gives the unique tip speed ratio for the maximum power output.

considering interactions between machines. The present experimental study aims to advance the understanding of the development of non-axisymmetric wakes of horizontal axis wind turbines (HAWT) further downstream to enable better modelling and active control of wind turbine interactions in arrays.

PIV images have been obtained in the wake of a two bladed HAWT from one to five diameters downstream at a range of yaw angles. The study can be considered as a fundamental study of the behaviour of wakes behind deflecting bodies, but also has a clear application to actively control and maximise the power output from wind farms. A possible feature of the result may be concluded from Fig. 1.

2. Experimental set up and data processing

Experiments were carried out in the 0.8m×1.2m MTL low turbulence wind tunnel at the Royal Institute of Technology (KTH), Stockholm, Sweden. A 0.25 m diameter two bladed model wind turbine (further details given in Alfredsson & Dahlberg (1979)) was positioned in the centre of the tunnel on a tower standing on the tunnel floor. The wind turbine was controlled using a generator and load circuit. Rotor frequency, torque and thrust were measured to obtain power and force curves for the wind turbine at different tip

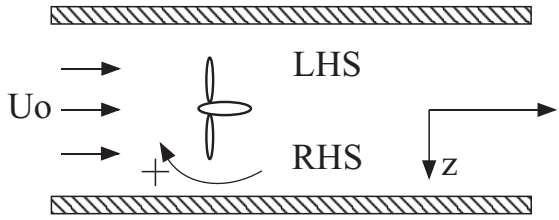

FIGURE 3. Experimental set-up, top view, showing yaw angle notation.

speed ratios (see Fig. 2). The tip speed ratio is the ratio between the tip velocity of the blade and the free-stream velocity. The turbine was then run at optimum tip speed ratio in a free stream wind velocity of 6.3 m/s. Using a laser sheet parallel to the flow, cutting through the centre of the turbine wake, PIV images were obtained at a series of positions - from approximately one diameter to five diameters - downstream of the rotor, at a number of different yaw angles. In the present study, a positive yaw angle indicates that the right hand side (RHS) blade of the turbine was yawed upstream when viewed in the downstream direction, see Fig. 3. Wake measurements were carried out for the following yaw angles [-30°, -20°, -10°, 0°, 10°, 20°, 30°] with each PIV image covering an area of approximately 0.17m×0.17m. At least 250 images were collected at each position with a spatial resolution of around 2.7 mm.

The PIV system included a two-cavity (400mJ each) Nd:YAG laser (Quanta Ray), with a wavelength, after frequency doubling, of 532 nm and pulse frequency of 14 Hz. The duration of the laser beam was 8.0 ns. A digital high-resolution Kodak ES 1.0 CCD-camera (1008×1018 pixel) was used. This was equipped with a 60 mm lens. The processor and software was delivered by DANTEC Measurement Technology, Denmark. The seeding was introduced downstream of the test section and re-circulated round the closed circuit wind tunnel producing uniform seeding in the test section. Seeding was achieved using smoke generated from 1,2-Propanediol diluted with 30-40% water with an approximate particle size of 2.0-2.5 μm volume median diameter (VMD). The PIV data post processing was evaluated using an in-house written Matlab code. The post processing used the Peak Value Ratio (PVR) - validation criteria, set to $\geqslant 1.2$. The velocity range was chosen up to 1.6× free-stream velocity in the streamwise direction and ±0.8× free-stream velocity in the spanwise direction. The measurements provided sufficient data for further analysis without the requirement for filling or smoothing.

3. Results and discussion

Figs. 4 and 5 show the composed velocity surface plots of the wake for a series of downstream positions of the wind turbine at zero and 30 degrees yaw respectively. The average velocity has been subtracted so the flow features can be seen more easily. In these particular data sets there was no data acquired along the centre line since the outer part of wake was of interest. The colour scale represents the sum of the velocity vectors, with red representing downstream and positive spanwise (to RHS) directed velocity components and, at the other end of the scale, blue denoting upstream and negative spanwise directed components. The resultant of the free-stream velocity only consists of the downstream component and is denoted by yellow, thus representing the mid range vector sum. The laser sheet was positioned parallel to the flow direction, thus cutting through the helical vortices trailing from the blade tips. The intersection between the laser sheet and the helical vortex is seen as a series of isolated vortices at approximately 0.6 diameters from the centre of the wake, diverging and becoming more erratic downstream as the wake expands and the vortices break down. The velocity decreases towards the centre of the wake but, as more of the free stream is drawn into the wake, this inner-wake flow deficit is reduced and the velocity increases towards the free-stream velocity. In the zero yaw case the wake travels straight downstream of the rotor, as expected. When the turbine is positively yawed the wake is deflected towards the LHS of the rotor. The inner wake deficit is less pronounced as the rotor is less effective in extracting the energy from the wind.

Fig. 6 shows a close up of the intersection between the laser sheet and one of the trailing vortices, with the velocity vectors superimposed onto the colour plot. This figure shows the presence of data close to the core of the vortex. However, the centrifugal force in the centre of the vortex excludes tracer particles from this part of the flow thus the velocity vectors are seen to reduce and shows one of the problems of PIV in highly circulating flows.

In Fig. 7 the average streamwise velocity profiles are presented for different downstream positions showing the wake deflection due to yawing the turbine [0° 10° 20° 30°]. The yawing effect is clearly shown. At approximately x/D=4.5, at 30 degrees yaw, the wake is deflected approximately 30% of the rotor diameter. In each velocity profile there is a systematic velocity excess of 5% of the free-stream velocity in the outer region, which is thought to be due to the solid blockage effect also corresponding to 5%. A similar result was seen in Alfredsson *et al.* (1980) when studying the wake downstream of a turbine.

Fig. 8 shows the skew angle of the centre of the wake, calculated by taking the midpoint of the wake and comparing to zero yaw, for different yaw angles. Comparison is made with results by Grant *et al.* (1997). Since the curves flatten off at higher yaw angles, the gain in deflection by going to higher yaw angles is minimal. The results by Grant *et al.* (1997), where a larger rotor with different blade profiles was used, shows slightly higher wake skew angles but the shape of the curve is the same.

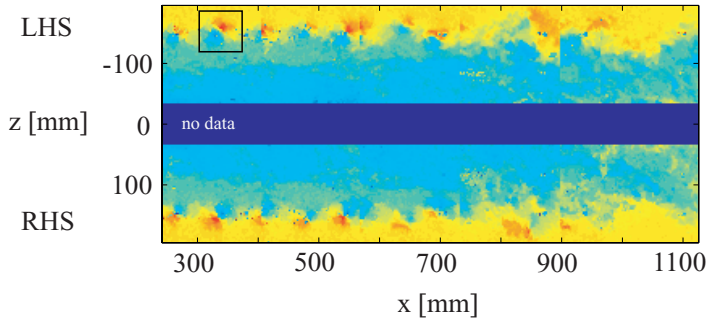

FIGURE 4. Composed velocity plot of a series of downstream image areas showing the wake development at zero yaw angle. The colour scale represents the sum of the velocity vectors, with red representing downstream and positive spanwise (to the RHS) directed velocity components and, at the other end of the scale, blue denoting upstream and negative spanwise directed components. The resultant of the free-stream velocity only consists of the downstream component and is denoted by yellow, thus representing the mid range vector sum.

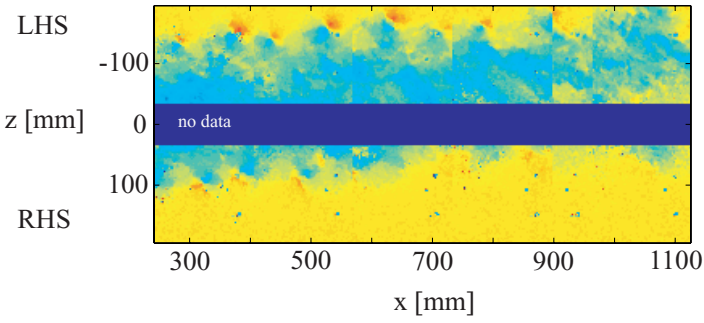

FIGURE 5. Composed velocity plot for 30 degrees yaw.

When analysing the wake development the comparison to field condition is always desirable but complicated. There are a number of non-dimensional groups of parameters that may influence the wake behaviour, such as the power coefficient, drag coefficient, tip speed ratio, aspect ratio (chord/blade length),

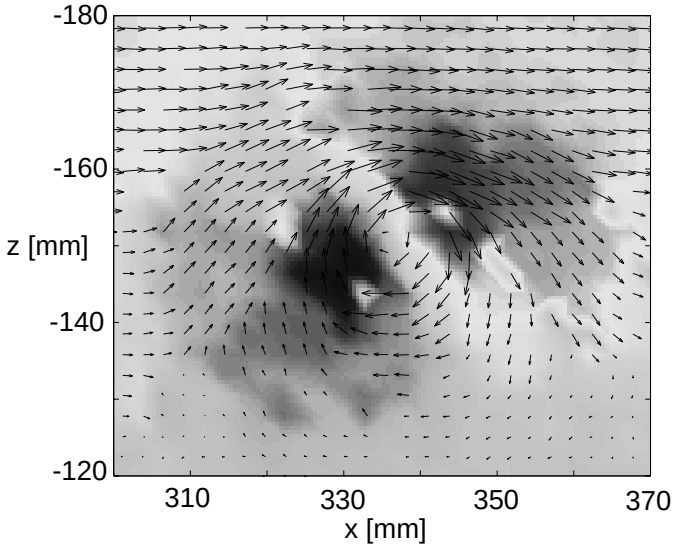

FIGURE 6. A close up of a vortex with velocity vectors, giving the center of the vortex. The upper part of the figure represents the free stream and the lower part the inner wake region.

Reynolds number etc. The ambient flow, which in nature is an atmospheric boundary layer, is of course also an important factor for the wake dispersion, especially the ambient turbulence level. The present study was performed at a low turbulence level and therefore the wake dispersion would be smaller than in nature. The strength and stability of the tip vortices is another important factor which may affect the spreading of the wake. However the qualitative feature of wake deflection would still be valid and future work will include free stream turbulence and mean shear gradients.

The application of this study to the active control of wind turbine wakes in wind farms is illustrated in Fig. 9 and Fig. 10. Here the wake streamwise velocity, expressed as a fraction of the free-stream velocity, is plotted versus yaw angle for a number of axial positions for a particular distance downstream. Only the streamwise velocity component is considered as the spanwise component in the outer part of the wake was negligibly small and in the inner part, where it was possible to contribute, was less than 10%. So, if we were to position a second turbine at this distance downstream from the first turbine, it would be desirable for the wind speed to be as near to the free stream as possible. The figure shows what yaw angle of the upstream turbine is required to give a particular wind speed at varies span positions with respect to the upstream turbine of a downstream turbine. For example, if the blade of the downstream

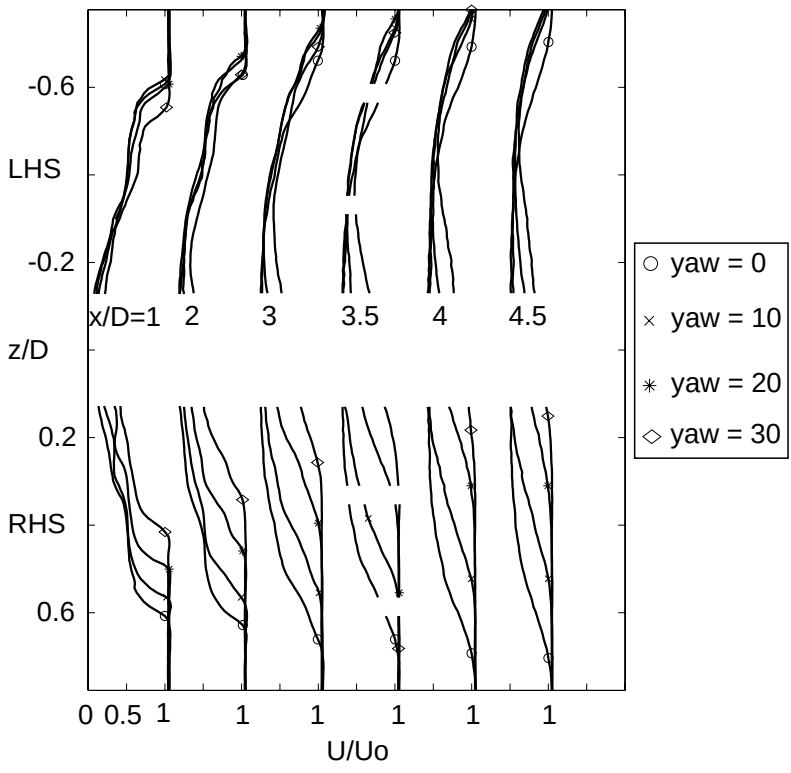

FIGURE 7. The mean velocity profiles of the streamwise flow component for different downstream positions and yaw angles [0° 10° 20° 30°].

turbine was directly downstream of the upstream rotor a free-stream velocity could be achieved by yawing the upstream rotor by 30 degrees. In reality this is unlikely to optimise the energy output from both turbines as yawing a turbine by 30 degrees will give a significant reduction in energy output. A more realistic example is if the downstream turbine was at a span position of 0.4. The upstream turbine could be yawed by 10 degrees to get 95% of the free stream, or by 20 degrees to get the free-stream wind velocity.

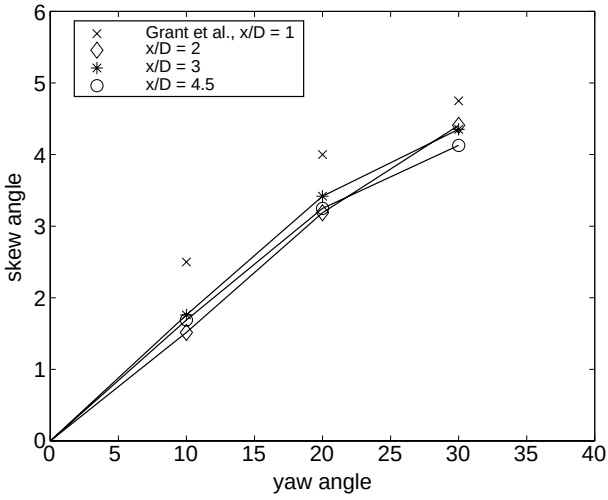

FIGURE 8. The wake skew angle at different downstream positions, calculated from the displacement of the midpoint between the two sides at 95% of the free-stream velocity.

4. Conclusions

The results presented show a clear picture of the wake of a wind turbine, both aligned into the wind and at a range of yaw angles, up to approximately 5 diameters downstream. The positions of the trailing tip vortices are shown and vortex dissipation downstream illustrated. When the turbine is yawed the wake is deflected and this effect seems to increase further downstream. The wake deflection effect in yaw will be used in continued studies to investigate the possibility of active control of the wake paths in wind farm applications and the feasibility of this has been illustrated in present study.

5. Acknowledgements

The authors would greatly acknowledge the Swedish National Energy Administration for financially supporting this project. The authors are also very thankful for the support of equipment and fruitful discussion with the staff at the Wind Energy Department at the Swedish Defence Research Agency (FOI/FFA) in Stockholm and finally thanks to the colleges and technicians at the Department of Mechanics at KTH.

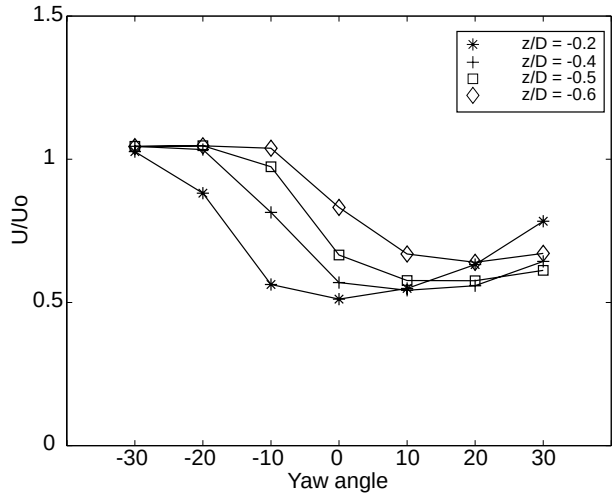

FIGURE 9. The essence of the wind tunnel tests. The influence on the streamwise velocity value, and thus a second wind turbine D, at a downstream position of x/D=4.5 from turbine C at different yaw angles. The parameter is the spanwise position (z/D) for turbine D, see Fig. 1.

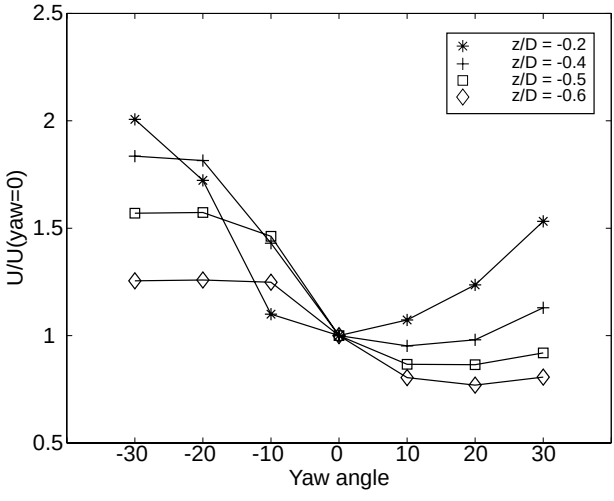

FIGURE 10. Figure 9 normalized with the data for zero yaw angle.

References

Alfredsson, P. H. & Dahlberg, J. Å. 1979 A preliminary wind tunnel study of windmill wake dispersion in various flow conditions. FFA Technical Note AU-1499, part 7.

Alfredsson, P. H. & Dahlberg, J. Å. 1981 Measurements of wake interaction effects on the power output from small wind turbine models. FFA Technical Note HU-2189, part 5.

Alfredsson, P. H., Dahlberg, J. Å. & Bark, F. H. 1980 Some properties of the wake behind horizontal axis wind turbines. In *Proc. Third Int. Symp. on Wind Energy Systems*, Copenhagen, BHRA Fluid Engineering, paper J5, pp. 469–484.

Clayton, B. R. & Filby, P. 1982 Measurement effects of oblique flows and change in blade pitch angle on performance and wake development of model wind turbines. In *Proc. 4th BWEA Wind Energy Conference*, Cranfield, BHRA Fluid Engineering, pp. 214–224.

Grant, I. & Parkin, P. 2000 A DPIV study of the trailing vortex elements from the blades of a horizontal axis wind turbine in yaw. *Exp. Fluids* **28**, 368–376.

Grant, I., Parkin, P. & Wang, X. 1997 Optical vortex tracking studies of a horizontal axis wind turbine in yaw using laser-sheet flow visualisation. *Exp. Fluids* **23**, 513–519.

Pedersen, T. F. & Antoniou, I. 1989 Visualisation of flow through a stall-regulated wind turbine rotor. *Wind Engng.* **13**, 239–245.

Ross, J. N. & Milborrow, D. J. 1985 Laser velocimetry applied to the study of model wind turbines. *Optical Measurements in Fluid Mechanics*, Inst. of Physics Pub. Inc. (ISBN: 0-85498-1683), Institute of Physics Conf. **77**, pp. 27–31.

Sforza, P. M., Sheerin, P. & Smorto, M. 1981 Three-dimensional wakes of simulated wind turbines. *AIAA J.* **19**, 1101–1107.

Smith, D. & Taylor, G. J. 1991 Further analysis of turbine wake development and interactive data. In *Proc. 13th BWEA Wind Energy Conference*, Swansea.

Vermeulen, P. E. J. 1980 An experimental analysis of wind turbine wakes. In *Proc. Third Int. Symp. on Wind Energy Systems*, Copenhagen, BHRA Fluid Engineering, paper J3, pp.431–450.

2

Paper 2

Potential improvement of wind turbine array efficiency by active wake control (AWC)

By J. Å. Dahlberg† and D. Medici‡

† FOI, Aeronautics Division, FFA, Department of Wind Energy Research,
SE-172 90 Stockholm, Sweden
‡ KTH Mechanics, SE-100 44 Stockholm, Sweden

Proc. European Wind Energy Conference, Madrid, 2003.

1. Introduction

Wind energy is of increasing importance in electrical power production. The key for even further enhancing its role is to make the cost per produced energy unit competitive with other sources. Common approaches to control and therefore to optimize the power output include tip speed variation, stall, variable blade pitch, and yaw. The aerodynamic efficiency is one side of the problem, the other being the interaction between two or more turbines. This paper focuses on the possible increase in power output from a wind farm using an Active Wake Control (AWC) method.

Comprehensive studies on the wake characteristics of single turbines are available in the literature. Comparisons between tunnel tests and full-scale turbines (e.g. Magnusson & Smedman (1999) Whale *et al.* (1996)) are a typical example. Near wake measurements (Grant *et al.* (1999), Magnusson (1999)) have been performed using, for example, hot wire and laser techniques. The airflow behind wind turbines has also been investigated (Alfredsson *et al.* (1980), Vermeulen (1980)). Studies of wakes by Ronsten *et al.* (1994) visualised the wake deflection when the turbine was yawed. Smoke was injected in the airflow at two positions at hub height such that the smoke trails touched the blade tip paths on both sides of the turbine. A photo taken from the test is presented in Fig. 1. The two-bladed turbine was yawed 30 degrees and operated close to maximum power. The vortices emerging from each blade passage are clearly visible. Note the vortex core path on each side. Both the sides of the wake are deflected upward, although the lower side more noticeably.

Numerical simulations on a porous surface were investigated also in yaw, based on the actuator disc theory, after measurements with no yaw in a wind tunnel (Sforza *et al.* (1981)). Blade element theory is very popular when dealing with rotor performance analysis. For yawed conditions, free wake models based on induction velocities and prescribed wake models have been used (Coton & Wang (1999)). Engineering models are also based on wind tunnel measurements (Schepers (1999)). For a more detailed discussion about single turbine studies, extensive review literature is available (Hansen & Butterfield (1993), McGowan

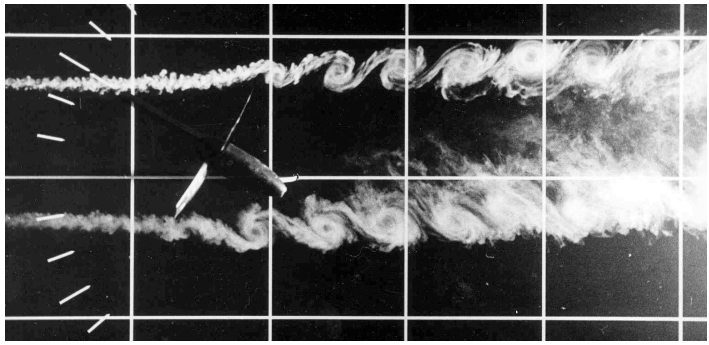

FIGURE 1. Flow visualisation of wake deflection from a turbine yawed 30° conducted at the Royal Institute of Technology (KTH), January 1987.

& Connors (2000), Leishman (2002)). Starting from a single wind turbine, the interaction between elements bundled into a wind farm has been investigated. The farm configurations depend strongly on the site, ranging from linear arrays to more complex geometries. Models for prediction of power production from wind farms have been implemented and compared with experiments (Landberg (1999)), as well models to calculate wind and turbulence characteristics inside a wind farm (Ivanova & Nadyozhina (1998)).

However, little information has been given about the mechanisms that influence the wake in connection with the power production. The aim of this study is to demonstrate the possibility of controlling the operational characteristics of a turbine and thereby controlling the development of the wake. Yawing the turbine implies that the relatively large thrust force, which essentially acts perpendicularly to the rotor plane, has been given an angle with respect to the wind. This side force causes the wake to change direction proportionally to its magnitude. Using controls installed in a large majority of wind turbines, the magnitude and direction can be modified. Pitch, tip speed ratio and yaw are believed to provide the desired changes on the wake and therefore on the output; consequently not only wake measurements will be discussed in the paper, but also power production from one wind turbine model as tested in a wind tunnel, and production from a bundle of turbines. The advantages will be reduced wake loads and increased power for the downstream turbine; the consequences for the controlled turbine will be reduced power and eventually increased loads. Although performance measurements for several pitch settings and tip speed ratio have also been made, the changes due to the modified magnitude of the thrust were not studied.

2. Experimental methods

An investigation by models in two wind tunnels was carried out to understand to what extent the development of the wake could be influenced by active wake control (AWC). The wake measurements were performed in the MTL (Minimum Turbulence Level) wind tunnel at KTH Mechanics. The tunnel test section is 1.2 m wide and 0.8 m high, for a total length of 7 m and an adjustable ceiling used to obtain a zero pressure gradient when empty. The coordinate system is x, y, z for the streamwise, wall-normal, and spanwise directions, respectively.

Used only in a first set of measurements, the 2-velocity component Particle Image Velocimetry (PIV) consists of seeding the flow with propylene glycol oil smoke and then taking a rapid sequence of two images with a CCD camera, while a pulsed laser sheet lights the flow. The PIV post-processing program was the Dantec software system FlowManager 2.12, by means of which the captured area of 1018×1008 pixels was divided in a mesh of 62×62 cells with no overlap. The cross correlation of the position of the smoke particles between the images resulted in a velocity vector in each of the cells, since the elapsed time between the two images was known. The side length of the captured images was 170 mm, giving a resolution for the velocity field of approximately 2.7 mm. A sketch of the experimental set-up can be seen in Fig. 2. A positive yaw angle was defined when the right hand side of the turbine as viewed from upstream, corresponding to positive z-values, was rotated downstream. Measurements were made in the horizontal (i.e. xz) plane; the camera was equipped with a 60 mm lens and fixed under the wind tunnel floor, looking up through a plexiglass panel. The flow was seen as coming from bottom to top of the captured area, therefore a positive yaw angle caused the flow to move toward the left side of the picture, i.e. to positive z-values.

The turbine was a 2-bladed model with a diameter (D=2R) of 250 mm, and the hub of 40 mm was large enough to accommodate a power generator. The turbine was placed in the middle of the test-section and the running point was chosen as the one giving the maximum power coefficient from the generator. The free-stream velocity as measured by a Prandtl tube in the beginning of the test section was 6.3 m/s. Approximately 250 images were taken for each downstream position (from 1 to 4.5 diameters) and each yaw angle (0°,–10°,–20°,–30°). This number of images was not enough to calculate reliable statistics, consequently only the mean velocity components were derived.

A second turbine model was built at the Aeronautical Research Institute (FOI) of Sweden: the blade was based on the Göttingen 417A airfoil, because this thin airfoil has good performance at low Reynolds numbers. The blades were produced in a mould of carbon fibres reinforced epoxy. The outer 77% of the blades were tapered such that the tip chord was 16 mm and the maximum chord at 12% radius was 27 mm. This gave a solidity (blade area/swept area) of 13%. Each blade was attached to a 23 mm diameter hub by means of a screw glued parallel to the 25% chord line, giving a total diameter of 180 mm.

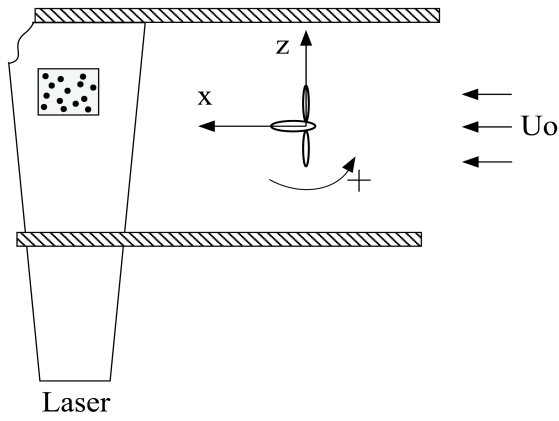

FIGURE 2. Experimental set-up for the PIV, top view. The region targeted by the camera under the floor is shown, with a sketch of the seeding particles (dots).

Any pitch angle could be fixed within an accuracy of 0.05°. The hub was then directly attached to the shaft of a DC motor having the same diameter.

The generator had a straight torque-current relationship that was determined through calibration, when the reaction torque on the housing of the generator was measured with strain-gauges. Three pair of blades were tested: the couple chosen for the experiment was the one giving the best performances in terms of power coefficient. A strain-gauge moment balance, close to the bottom of the 180 mm support, was used to measure the streamwise force and therefore the thrust coefficient. For this measure it was assumed that the resultant of the forces acting on the blades was located in the centre of the rotor, with an accuracy considered acceptable for non-yawed conditions.

Power (P) and thrust (T) as function of rotational speed have been measured in the MTL wind tunnel, using the wind turbine model presented above; the coefficients were defined as:

$$C_P = \frac{P}{\frac{1}{2}\rho\pi R^2 U_\infty^3} \tag{1}$$

$$C_T = \frac{T}{\frac{1}{2}\rho\pi R^2 U_\infty^2} \tag{2}$$

$$\lambda = \frac{\Omega \cdot R}{U_\infty} \tag{3}$$

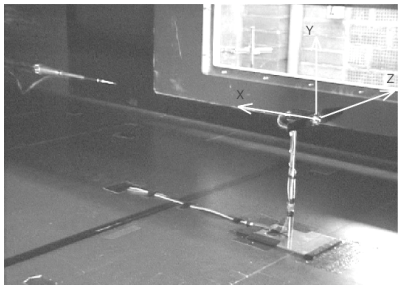

FIGURE 3. Experimental set-up for the hot-wire measurements. The reference axes are marked.

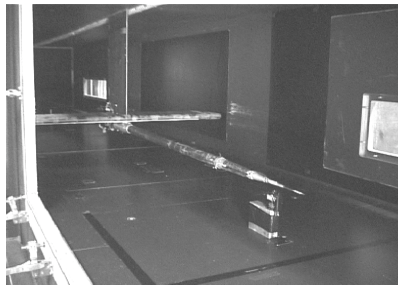

FIGURE 4. Traversing system and probe. The laser distance meter used to check the system vibrations is visible under the probe.

where Ω is the angular velocity and λ the tip speed ratio. The velocity wakes were then investigated with hot-wire anemometry. A picture of the experimental set-up is shown in Fig. 3. The X-wire probe was built for the experiment and connected to the traversing system in order to have five degrees of freedom. As can be noticed in Fig. 4, the probe was placed at one end of a shaft to minimize the disturbances. On the other hand, this reduced the maximum measurable distance to 15 diameters downstream of the turbine. The prongs of the probe were edged to minimize the disturbances with the flow and their separation was approximately 1 mm, which was also the side length of the cubic measurements volume. The platinum wires were 5 μm in diameter. The velocity components of interest (axial and radial) were the ones lying on the xz-plane, which therefore was the plane containing the wires. With a pitch angle for the two blades of 8°, three velocities were tested: 5, 8, 11 m/s at a constant thrust coefficient. Differencing the pitch angle to 7°/9° and 6°/10° between the two blades, additional sets of data were captured at 8 m/s. Data were acquired for 30 seconds at 6 kHz in each grid point for all the investigated conditions.

For the two lowest velocities tested, the anemometer voltages at the wake centreline were below the minimum calibration point. Since the two 5th degree polynomials used for the fitting of the values cannot be used outside the calibration velocities, a different approach was considered. The calibration points for the X-wire probe ranged between 3 m/s and 15 m/s, the seven angles between ±30°. The anemometer voltages that had in common the probe calibration angle were interpolated with the modified King's law. Thanks to the nature of the Kings law, the expected voltage at 1 m/s was extrapolated and inserted

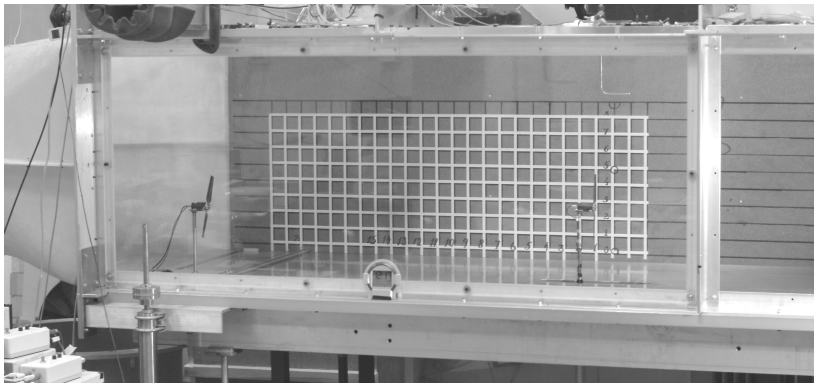

FIGURE 5. The test section of the LT5-II wind tunnel with two turbines mounted. The wind is blowing from right to left. The right turbine is fixed whilst the left turbine can be traversed from side to side.

as a calibration point. The polynomials so obtained could then be used in the new range 1 m/s to 15 m/s.

The power wakes measurements, expressing the power relatively to undisturbed conditions, were conducted in the LT-5, NPL-type wind tunnel at FOI. The tunnel (Fig. 5) has a 2.5 m long test section with a cross-section of 0.9×0.675 m and a velocity range from 5 m/s to 16 m/s. The wind speed in the centre of the test section was measured as the difference between the total pressure in the contraction and the averaged static pressure from four taps, two located upstream of, and two downstream of, the test section. The purpose of measuring the static pressures both up- and downstream of the turbine is to take the wake blocking effect into account when estimating the wind-speed.

By traversing a turbine through the wake of an upstream turbine at a fixed streamwise position in the test section, the interactions have been examined. The upstream turbine was positioned in the centre of the wind tunnel at fixed distances of 3, 5, 7 and 9 diameters. This model was yawed in 10° steps from –30° to +30°. The test was carried out such that the upstream turbine was operating at a fixed tip speed ratio, which gave nearly optimum C_P. The traversing turbine was as well connected to a load circuit, which for uniform flow would have kept the tip speed ratio constant. The downstream turbine was slowly traversed back and forth during 9 minutes, which enabled the turbine to complete four sweeps. All relevant data were continuously recorded at 17 Hz. The processing of data involved the conversion to physical values and sorting the data into 1 cm bins, with the position of the traversing turbine as the

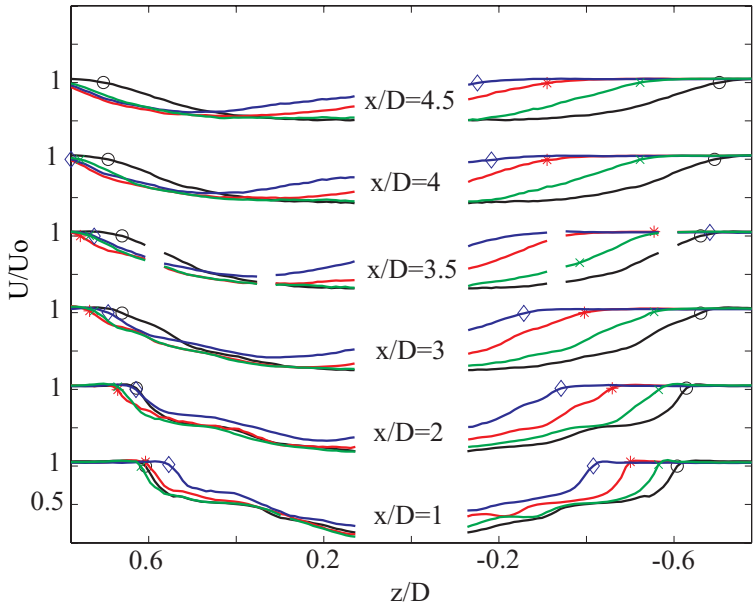

FIGURE 6. Mean velocity profiles (PIV), axial component. Different yaw angles are investigated: 0° (◯), +10° (×), +20° (∗) and +30° (◇).

independent variable. The C_P values in each bin were normalised with the corresponding C_P value for undisturbed conditions.

Slowly rotating the turbine back and forth between –35° and +35° and continuously recording the data was the method used to calculate the reduction in power due to yaw operation. A positive yaw angle was defined when the right hand side of the turbine, corresponding to positive z-values, was rotated upstream. The turbine was connected to a load circuit that kept the turbine in near constant TSR operation.

3. Results

The data can be divided into three main groups: measurements performed on one wind turbine, on the interactions between two turbines, and finally on a model describing a wind farm of 6 elements. The wake measurements were limited to the single turbine test, the performances and force data to all the cases.

Single turbine study: a wind turbine working in yawed conditions ranging from 0° to ±30° was investigated with PIV. The displacement of the wake is plotted in Fig. 6 for different yaw angles. From the velocity field, once the

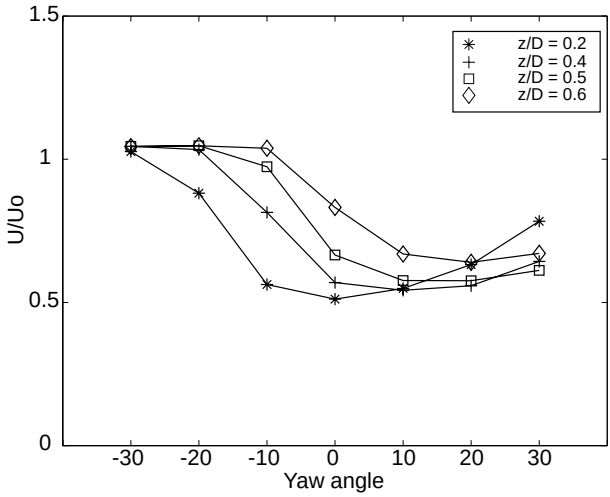

FIGURE 7. Velocity gains in a fixed position as function of the yaw angle, for different spanwise positions.

downstream position was chosen and a point at a known spanwise distance from the centre of the turbine was selected, the local velocity value could be calculated, as shown in Fig. 7. In this case the relative velocity value as a function of the yaw angle is shown for x/D=4.5.

The operational conditions such as pitch angle and tsr for the 180 mm diameter wind turbine were selected to give a thrust, and thereby a wake, which resembled conditions for full-scale turbines. A more detailed description involving two turbines will be given in the next section. The performances of the models were measured at constant wind speed and by manually loading the turbine with different resistors. For each load-case the wind speed, rotational speed, torque and thrust were recorded for 10 seconds. The power coefficient C_P and thrust coefficient C_T versus tip speed ratio could be plotted as function of the blade pitch angle. The performance characteristics for the turbine model can be seen in Fig. 8 and Fig. 9. The power coefficient C_P is relatively low, whilst the thrust values expressed as C_T reaches values that are realistic for full-scale turbines. The low C_P values are probably caused by non-optimal airfoil performance at low Reynolds number with a relatively high airfoil drag. Some reduction in performance can also be attributed to the non-twisted blades. As regarding the performances in yaw, the data sorted into two degree bins are presented in Fig. 10 with the pitch set to 8° and the turbine operating close to maximum C_P. The following expression:

$$\frac{P}{P_0} \;=\; [\cos(\beta - \beta_0)]^{exp} \tag{4}$$

was fitted to the binned data and showed to give a good representation of the power versus yaw angle characteristics.

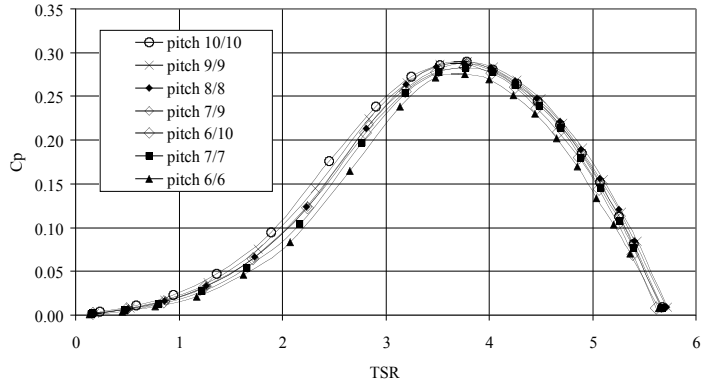

FIGURE 8. Power coefficient C_P versus λ (TSR) for different pitch settings. Note that the C_P curves with different pitch settings on the two blades, 7°/9° and 6°/10°, are very similar to the curve with the pitch set to 8° on both blades (8°/8°).

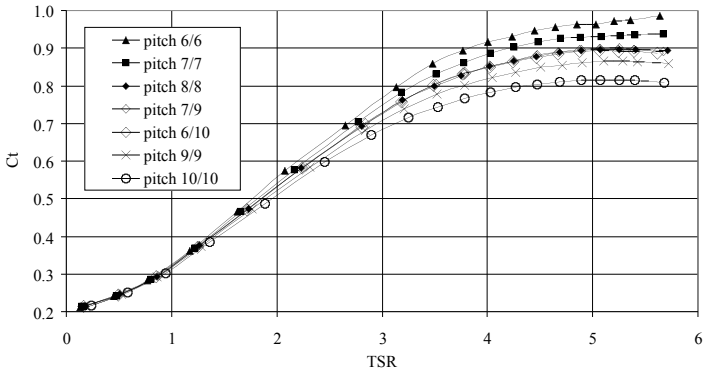

FIGURE 9. Thrust coefficient C_T versus λ (TSR) for different pitch settings. Note that the C_T curves with different pitch settings on the two blades, 7°/9° and 6°/10°, are very similar to the curve with the pitch equals to 8° on both blades (8°/8°).

The exponent here used will now on be referred to as the cosine-loss-exponent. The relative power P/P_0 was defined as the ratio between the actual performance and the performance in non-yawed condition. As indicated in Table 1, the power coefficients and fitted exponents changed for different pitch settings and operational conditions. The offset values β_0 varied in the range 0.2°-0.7° and the effect was probably due to the presence of the tower. The exponents found from these tests are believed to be too high to represent full-scale conditions. One reason could be that the load circuit did not manage to

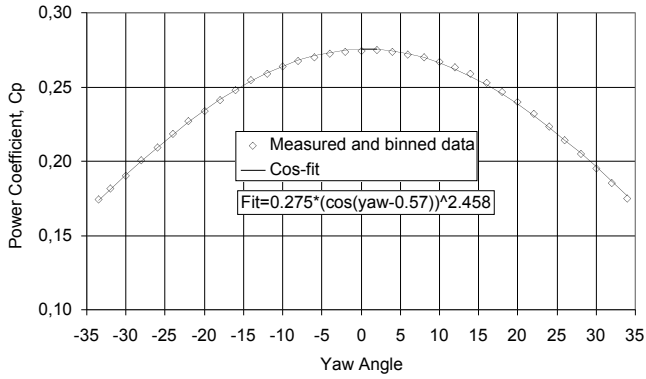

FIGURE 10. C_P as function of yaw for turbine model with pitch set to 8° and operating at C_{Pmax}.

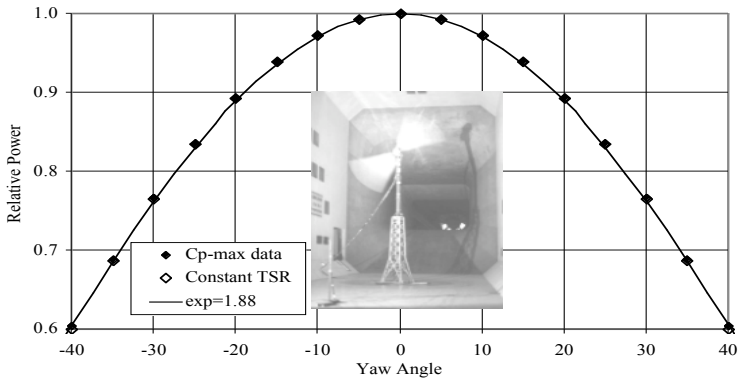

FIGURE 11. Relative power vs. yaw angle, derived from tests on a 5.35 m diameter wind turbine in CARDC 12×16 meters low speed wind tunnel 1994, China (from Ronsten *et al.* (1994)).

keep the tip speed ratio at optimum C_P for the yawed condition. The exponent for the PIV experiment was 2, whereas a similar yaw test carried out on a 5.35 m diameter turbine gave a corresponding exponent of 1.88. The result from the mentioned experiment is recalled in Fig. 11.

The wake was also measured with hot wire anemometry in the axial (u) and radial (w) velocity components, as shown in Fig. 12 and Fig. 13. In Fig. 14 the radial component for downstream positions up to 9 diameters and for 8 m/s are described. The rms for the axial velocity is presented in Fig. 15, up to 5 diameters downstream. The profiles above x/D=5 are decreasing in absolute value,

Pitch angle	λ (TSR)	Power Coefficient	fitted exponent	note
6	3.14	0.233	2.316	
6	3.70	0.264	2.322	C_{Pmax}
6	4.18	0.246	2.254	
8	3.18	0.252	2.475	
8	3.72	0.274	2.458	C_{Pmax}
8	4.21	0.257	2.541	
10	3.21	0.259	2.639	
10	3.75	0.275	2.684	C_{Pmax}
10	4.21	0.250	2.894	

TABLE 1. Turbine parameters.

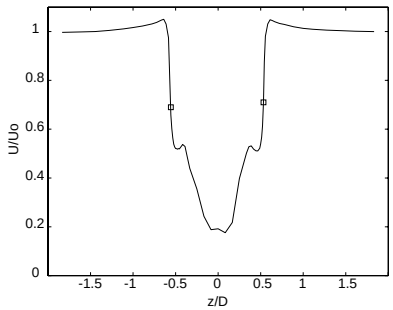

FIGURE 12. Axial mean velocity component at U_0=8 m/s and x/D=0.5. The points marked with the squares are mid-way from the overshoot and the local minimum at approximately z/D=±0.555.

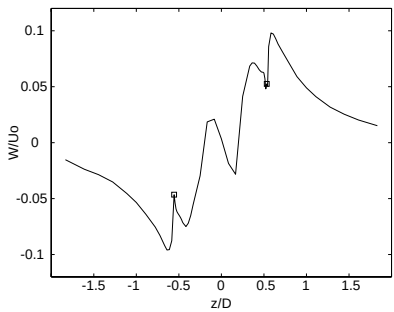

FIGURE 13. Radial mean velocity component at U_0=8 m/s and x/D=0.5. The squares identify the centre of the vortices. The profile has been shifted 0.015 down.

but not changing in shape. The free-stream velocity was used to normalise the quantities.

The turbine was run at essentially the same thrust coefficient also during the active wake control investigations. The blade pitch angle was differentiated between the two blades, first to 7° and 9°, and then to 6° and 10°. The axial velocity was affected by the control, as plotted in Fig. 16, more noticeably in the centre.

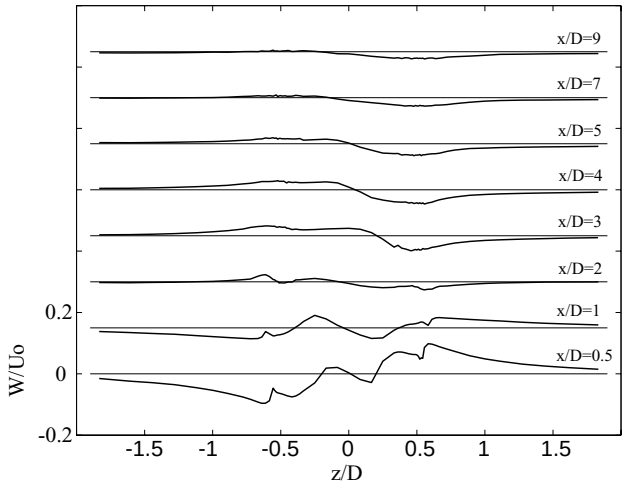

FIGURE 14. Spanwise mean velocity profiles for several downstream positions. The change of sign is evident from two diameters downstream. The profiles for U_0=5 m/s and U_0=11 m/s are similar.

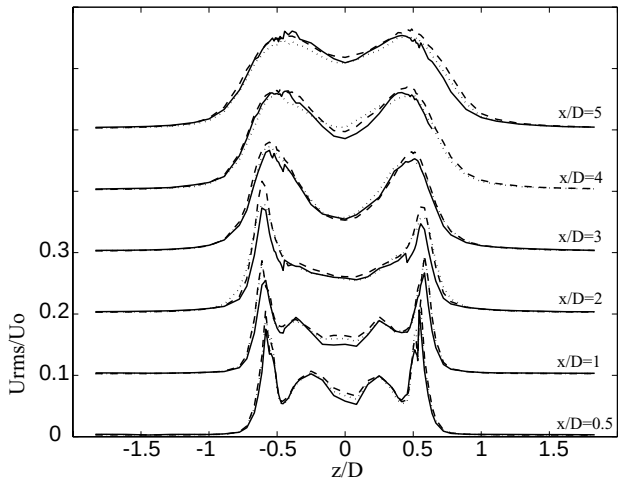

FIGURE 15. u_{rms} profiles from x/D=0.5 to x/D=5: solid (5 m/s), dotted (8 m/s), and dashed line (11 m/s).

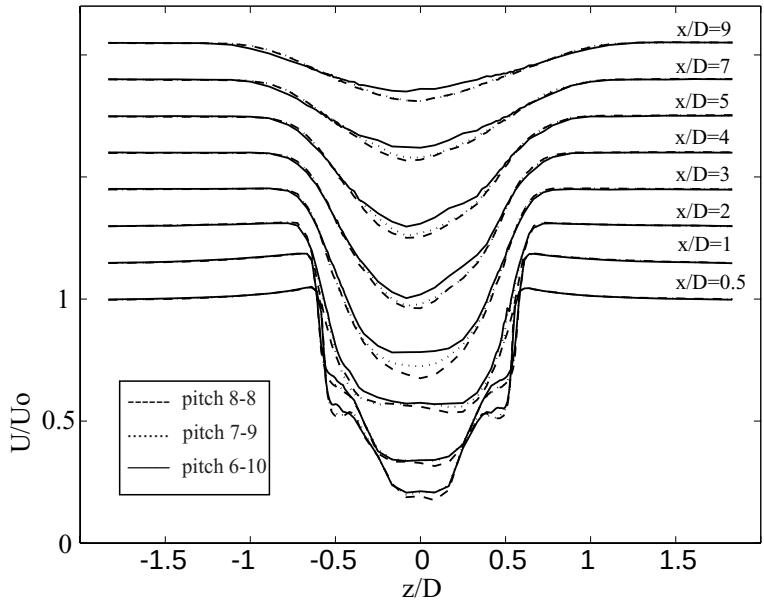

FIGURE 16. Streamwise mean velocity component. The pitch angles for the two blades are 8°/8° (dashed), 7°/9° (dotted), and 6°/10° (solid line).

Two turbines study: the relative power for one turbine, i.e. the power output normalised with the power for the undisturbed conditions, has been used to quantify the interferences caused by the wake from an upstream turbine. As mentioned above concerning the choice of the running conditions for the turbines, a comparison of the power wakes from the models and wake data measured at a small wind farm in Alsvik, consisting of four 180 kW turbines, are presented in Fig. 17. The farm is situated close to the shoreline and the flow comes from the open sea. This gives a very low turbulence intensity of about 5%, based on 1-minute data. The layout of the farm is such that one turbine is exposed to wakes from upstream turbines that are separated by 5, 7 and 9.5 diameters, depending on the wind direction. Data from the power wake survey for 3 and 9 diameters are shown in Fig. 18 and Fig. 19.

Wind farm model: the power wakes resulting from traversing the wind turbine, have been used to demonstrate the possibility of increasing the array efficiency by using AWC in a simulated wind farm. Five turbines were equally distributed on a circle around a centred turbine as depicted in Fig. 20, where the wind direction was considered clockwise from the top-to-bottom line. The layout of the wind farm was selected such that essentially no more than two

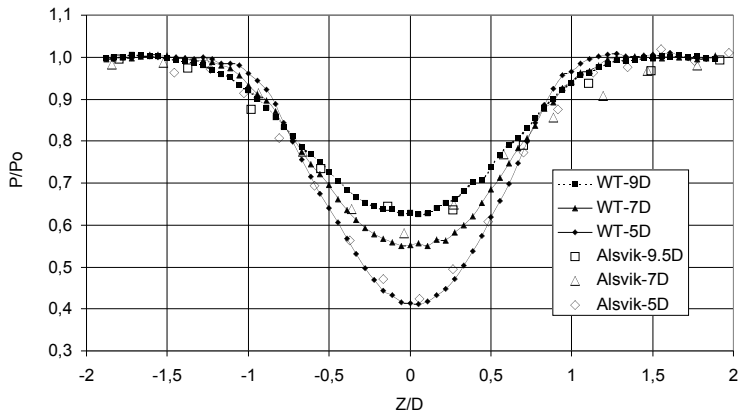

FIGURE 17. Comparison between LT5 measurements (wind tunnel, WT) and Alsvik power curves.

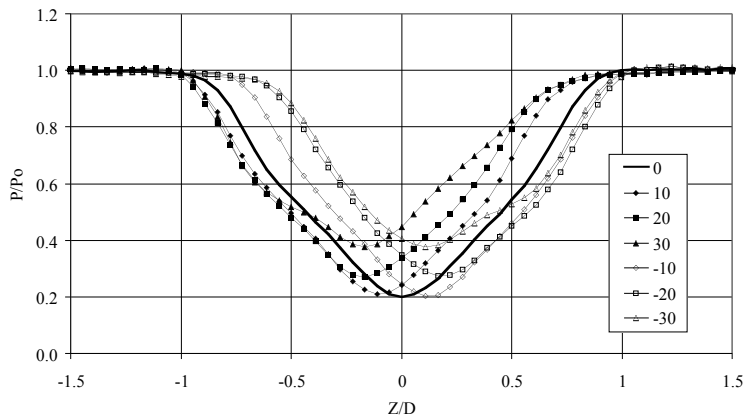

FIGURE 18. Relative power versus relative side position for the downstream turbine. The power-wakes are obtained by traversing the downstream turbine through the wake from the upstream yawed turbine. The turbine distance is 3D.

individual pairs of turbines were influencing each other simultaneously. This enabled direct interpolation in the measured database matrix for yaw operation from –30° to +30° and downstream distance between 3 and 9 diameters. Wind direction sector, direction steps, radius of the circle as well as cosine-loss-exponent were given as input to the calculations. For each wind direction the relative power of each turbine was determined by interpolation in the database. This was done with and without AWC. When AWC was used, the optimum yaw

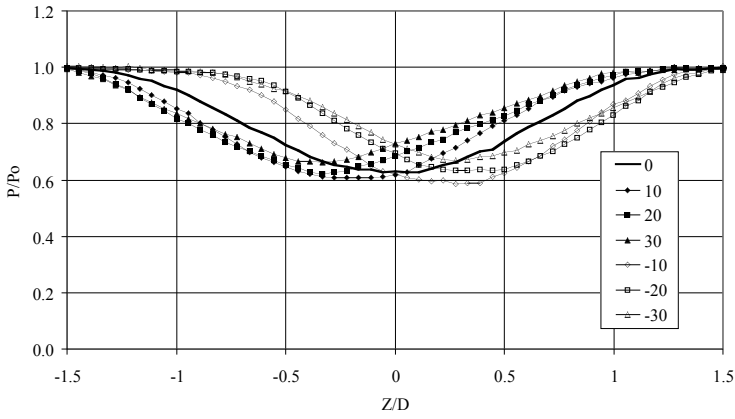

FIGURE 19. Relative power versus relative side position for the downstream turbine. The power-wakes are obtained by traversing the downstream turbine through the wake from the upstream yawed turbine. The turbine distance is 9D.

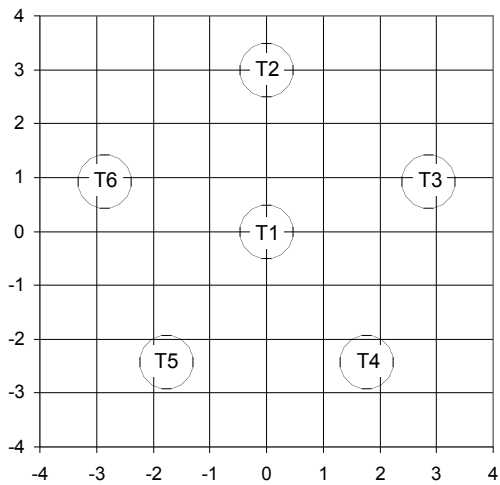

FIGURE 20. Wind farm used for the simulations.

angle was searched to give the maximum total power for all turbines involved. The optimisation process took into account the increase in power for the downstream turbine(s) due to AWC as well as the reduction in power for the yawed turbine. The calculations were performed for circle radii (distance between turbine T1 and T2:T6) of 3, 4 and 5 diameters and cosine-loss-exponents in 0.5 steps from 0 to 3. Fig. 21 exemplifies, for conditions when T6 operated in

the wake from T2, the reduction in power for the yawed turbine (T2) as well as the increase for the downstream turbine (T6) with AWC. In this example the radius in the farm is 3 diameters, the linear distance between the turbines is approximately 3.5D, and the cosine-loss-exponent is set to 2. The optimum yaw angle for T2 can also be seen in Fig. 21. The corresponding percentage gain for the two turbines is presented in Fig. 22. Maximum gain exceeds 11%. Note that the curves in these figures are not fully symmetric. This is caused by the direct use, by linear interpolation, of the measured data. The detailed percentage gain in power for the whole farm, for one fifth of the wind rose, and at different cosine-loss-exponents is presented in Fig. 23. The values for exp=0 give the total available increase, since no losses for the upstream turbines were considered. Reasonable values of the exponent for full-scale turbines are believed to fall in the 1.5-2.0 range.

In Table 2 the possible increase in power for the whole farm exposed to equally distributed wind directions is shown. The total averaged gain in energy yield is then 2 to 4% for the supposed full-scale exponents. Turbines extract about 75% of the total energy below the rated power; therefore AWC could be applied during most of the production time in order to improve the overall efficiency of the park. It is obvious that there is more to gain at shorter distances for a given yaw angle, since the velocity/power deficit decreases with distance. This is the reason why the shorter turbine separation gives the highest gain.

radius	exponent	no AWC	AWC	% gain
3	0	0.836	0.910	8.9
4	0	0.888	0.943	6.3
5	0	0.918	0.961	4.7
3	1.5	0.836	0.868	3.9
4	1.5	0.888	0.914	3.0
5	1.5	0.918	0.939	2.3
3	2	0.836	0.862	3.1
4	2	0.888	0.910	2.5
5	2	0.918	0.936	1.9
3	2.5	0.836	0.857	2.5
4	2.5	0.888	0.907	2.2
5	2.5	0.918	0.933	1.7
3	3	0.836	0.854	2.2
4	3	0.888	0.905	1.9
5	3	0.918	0.932	1.5

TABLE 2. Array efficiency.

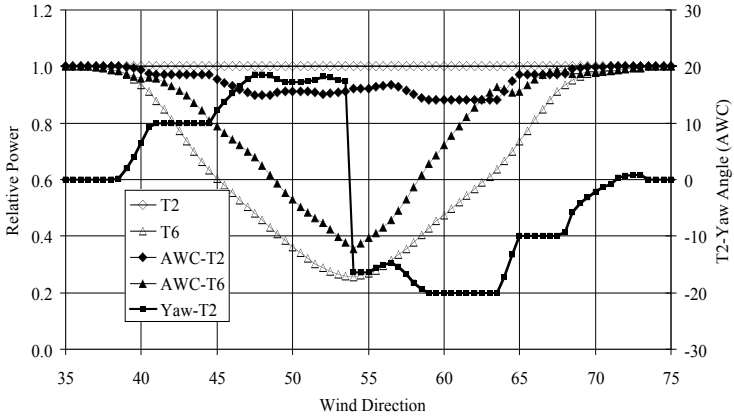

FIGURE 21. The relative power from T2 and T6 is plotted. The yaw angle for T2 was applied by the AWC code. The distance between the turbines is 3.5D and an exponent 2 was used as cosine-loss-coefficient.

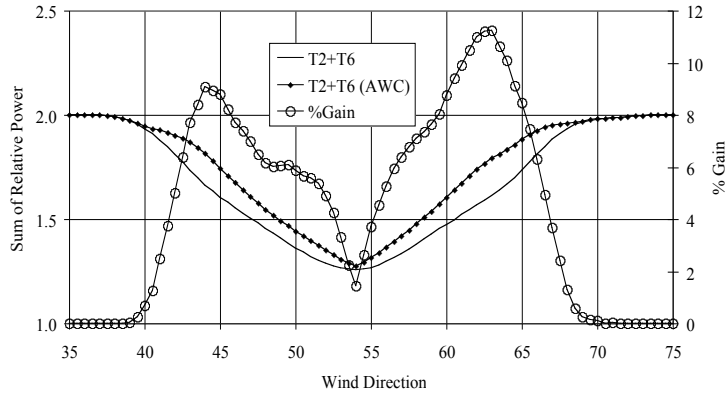

FIGURE 22. Relative power with/without AWC, and gain as from Fig. 21. The radius of the wind farm is 3D and the cosine-loss exponent is 2.

4. Discussion

This paper deals with the possible effects of active wake control on wind turbines, studied experimentally in wind tunnels. An aspect that should also be considered when dealing with wind turbine wakes is the tip vortex path. A

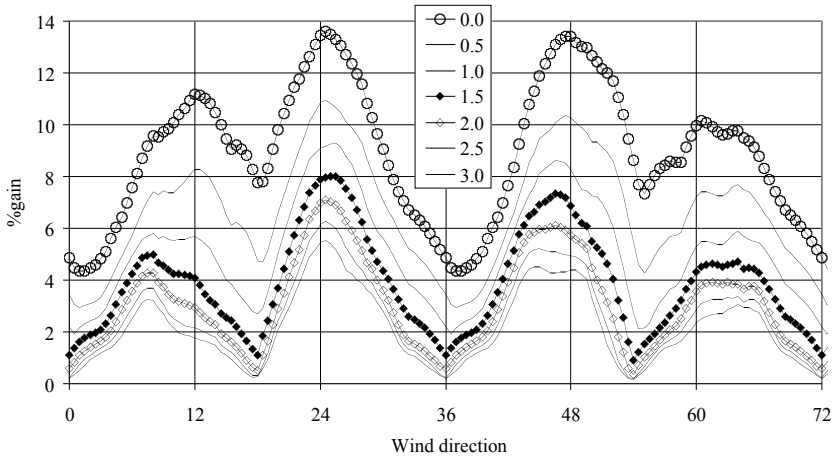

FIGURE 23. Power increase for the entire wind farm, with assumed losses due to yaw operation. The radius of the wind farm, i.e. the radius of the circle on which turbines T2 to T6 are positioned, is 3D.

clear result from the hot wire measurements of the wake (Fig. 12 and Fig. 13) is that the position of the centre of the vortex has, already at 0.5 diameters, moved out with respect to the blade tip. The centre can be detected not only as the mid-point between the overshoots (downwind and upwind) in the axial velocity, but also as a sudden dip in the radial velocity. It can be noted from Fig. 14 that the wake is first expanding, identified as a radial velocity directed outwards due to the effect of the reduction of speed through the turbine. Soon however the entrainment of flow from the free-stream to the wake takes over. The position corresponding to two diameters is probably when the vortex effect is less strong than the turbulence created by the wake: not only the peak identifying the centre of the vortex has almost disappeared, but also the radial velocity changes sign.

The position of the vortex can be of crucial importance when applying AWC, since structural problems might be taken into account when choosing the control parameters. As seen in Fig. 15, the vortex positions at approximately z=$\pm$100 mm for x/D=0.5 correspond to a very high peak in the rms values. It is believed that the two inner peaks are due to the higher velocity gradient in the wake, and then they merge with the vortex peaks between two and three diameters. It can also be observed, both from the smoke visualization in Fig. 1 and from a spectral analysis, that this distance corresponds to the grouping in pairs of the vortices, with no free-stream turbulence.

The development of the wake is mainly affected by the magnitude and direction of the thrust force. The tip speed ratio and blade pitch angle control the magnitude. If the pitch angle is fixed, a change in the TSR always produces a change both in the power and in the thrust coefficients, as seen in Fig. 8 and Fig. 9. On the other hand, if the average blade pitch angle of the blades is kept constant (as for the 8°/8°, 7°/9°, and 6°/10° cases), the coefficients are unaffected. However, although the thrust coefficient is the same, the shape of the wake can be different, as can be seen in Fig. 16. The AWC applied to the pitch had a consistent effect on the velocity profiles: the larger the pitch difference between the blades, the smaller the velocity deficit in the centre of the wake. Since the thrust coefficient was the same, the total area derived from the momentum thickness should be the same. At a larger radius, even a very small velocity error has a large effect on the integral; therefore the calculations were not performed. On the other hand, it can be seen that the velocity deficit is higher in the controlled case (with a different pitch angle on the blades) for the outer region, compensating for the decrease in the centre of the wake.

In yaw, the other control method analyzed, a dependence on the model used for the experiment is noticed for the power output, Fig. 10 and Fig. 11. The cosine-loss-exponent is still unknown for full-scale turbines, but the loss is lower than that expected from theoretical considerations (the power should be proportional to the cube of the velocity component perpendicular to the actuator disc). The velocity profiles obtained with PIV, Fig. 6, show how large the displacement of the wake in yawed conditions can be. The nature of the data allows to know the velocity profiles in any position from 1 to 4.5 diameters with a step of 2.7 mm. It can also be noted how effective the AWC is on the side of the turbine with the blade moved upstream, as shown in the introduction from the smoke visualization. For example at 4.5D and 20° of yaw, the wake has been moved a distance approximately 30% of the diameter. If a downstream turbine was shadowed by the wake of the non-yawed turbine, the same control could have avoided any interaction. Fig. 7 clearly states how, once the point is selected, the upstream turbine should be yawed to obtain a desired velocity change. From Fig. 18 and Fig. 19, the yawing of the upstream turbine can give a power gain for the downstream turbine of, for instance, 30% for 20° and z/D=0.5. The interesting quantity is the relative total gain, which takes into account also the power loss from the yawed turbine. In Fig. 21 and Fig. 22 it is shown that the gain can be of the order of 10% for the controlled case, if applied to two wind turbines. In this case, the considered downstream distance is three diameters and the cosine-loss-exponent is 2. For the wind farm of radius 3D simulated in the study, the maximum power gain for favourable wind directions ranged between 5% and 8% if a cosine-loss-exponent representative for full-scale turbines is considered (Fig. 23). The cosine-loss-exponent is a crucial data for the final result, but it is believed that a value of 1.5-2 can be applied for full-scale turbines.

Models resembling the running conditions of full-scale turbines have been successfully used to demonstrate that array efficiency can be improved by using Active Wake Control. The wake has been modified in its shape using pitch control, and deflected using yaw. It should be noted that this study has not addressed any fatigue or load issues. The turbine in yawed conditions undergoes larger stresses, but the downstream turbine can be relieved from the loads due to the presence of the oncoming wake.

References

Alfredsson, P. H., Dahlberg, J. Å. & Bark, F. H. 1980 Some properties of the wake behind horizontal axis wind turbines. In *Proc. Third Int. Symp. on Wind Energy Systems*, Copenhagen, BHRA Fluid Engineering, paper J5, pp. 469–484.

Coton, F. N. & Wang, T. 1999 The prediction of horizontal axis wind turbine performance in yawed flow using an unsteady prescribed wake model. In *Proc. Instn. Mech. Engrs.*, **213** Part A, pp. 33–43.

Grant, I., Mo, M., Pan, X., Parkin, P., Powell, J., Reinecke, H., Shuang, K., Coton, F. & Lee, D. 1999 An experimental and numerical study of the vortex filaments in the wake of an operational, horizontal-axis, wind turbine. *J. Wind Engng. Ind. Aerodyn.* **85**, 177–189.

Hansen, A. C. & Butterfield, C. P. 1993 Aerodynamics of horizontal-axis wind turbines. *Annu. Rev. Fluid Mech.* **25**, 115–149.

Ivanova, L. A. & Nadyozhina, E. D. 1998 Wind flow deformation inside the wind farm. *J. Wind Engng. Ind. Aerodyn.* **74-76**, 389–397.

Landberg, L. 1999 Short-term prediction of the power production from wind farms. *J. Wind Engng. Ind. Aerodyn.* **80**, 207–220.

Leishman, J. G. 2002 Challenges in modelling the unsteady aerodynamics of wind turbines. *Wind Energy* **5**, 85–132.

Magnusson, M. 1999 Near wake behaviour of wind turbines. *J. Wind Engng. Ind. Aerodyn.* **80**, 147–167.

Magnusson, M. & Smedman, A.-S. 1999 Air flow behind wind turbines. *J. Wind Engng. Ind. Aerodyn.* **80**, 169–189.

McGowan, J. G. & Connors, S. R. 2000 Windpower: a turn of the century review. *Annu. Rev. Energy Environ.* **25**, 147–197.

Ronsten, G., Dahlberg, J. Å., Giuqing, J. & Dexin, H. 1994 An experimental investigation of the performance and wind tunnel wall interference for a wind turbine operating in yaw. FFA scientific report, FFA TN 1994-13.

Schepers, J. G. 1999 An engineering model for yawed conditions, developed on the basis of wind tunnel measurements. AIAA paper 99-0039, 18th ASME Wind Energy Symp., and 37th AIAA, Aerospace Sciences Meeting and Exhibit, Reno, also published in *Collection of Technical papers* (A99-17151 03-44).

Sforza, P. M., Sheerin, P. & Smorto, M. 1981 Three-dimensional wakes of simulated wind turbines. *AIAA J.* **19**, 1101–1107.

Vermeulen, P. E. J. 1980 An experimental analysis of wind turbine wakes. In *Proc. Third Int. Symp. on Wind Energy Systems*, Copenhagen, BHRA Fluid Engineering, paper J3, pp.431–450.

Whale, J., Papadopulos, K. H., Anderson, C. G., Helmis, C. G. & Skyner, D. J. 1996 A study of the near wake structure of a wind turbine comparing measurements from laboratory and full-scale experiments. *Solar Energy* **56**, 621–633.

3

Paper 3

Measurements on a wind turbine wake: 3D effects and bluff-body vortex shedding

By D. Medici and P. H. Alfredsson

KTH Mechanics, SE-100 44 Stockholm, Sweden

Accepted for oral presentation and Proc. at The Science of Making Torque from Wind, Delft, 2004.

The velocity field in the wake of a two-bladed wind turbine model (diameter 180 mm) has been studied under different conditions using a two-component hot-wire. All three velocity components were measured both for the turbine rotor normal to the oncoming flow as well as with the turbine inclined to the free stream direction (the yaw angle was varied from 0 to 20 degrees). The measurements showed, as expected, a wake rotation in the opposite direction to that of the turbine. A yawed turbine is found to clearly deflect the wake flow to the side showing the potential of controlling the wake by yawing the turbine. An unexpected feature of the flow was that spectra from the time signals showed the appearance of a low frequency fluctuation both in the wake and in the flow outside. This fluctuation was found both with and without free stream turbulence and also with a yawed turbine. The Strouhal number of that frequency was independent of the free-stream velocity or turbulence level, but the low frequency was only observed when the tip speed ratio (or equivalently the thrust coefficient) was high. The shedding frequency changes also with the yaw angle. This is in agreement with the idea that the turbine shed structures as a bluff body. The phenomenon, noticeable in all the velocity components, was further investigated using a two point cross-correlation.

1. Introduction

The wake development behind wind turbines is of considerable practical interest, it both gives information on power losses in turbine parks as well as increased turbulence levels which may be affecting flow induced rotor loads. For wind engineering purposes the main interest is in the near wake region, say up to $10D$, where D is the turbine diameter, downstream the turbine. The main characteristics of the near wake are the mean velocity deficit and the tip vortices shed by the blades forming two (or three for a three bladed turbine) spiral vortices downstream the turbine. For a recent comprehensive review on wind turbine wakes the reader is referred to Vermeer *et al.* (2003).

The flow (wake) behind axis-symmetric bodies has been studied for long times, however the most interest has been focused on the far wake development

(see e.g. Johansson *et al.* (2003)). Much less work has been focused on the near wake region. It is well known that two-dimensional bodies (i.e. cylinders or plates) give rise to large scale vortex shedding, however a similar type of large scale shedding may also appear behind three-dimensional blunt bodies. For instance Bevilaqua & Lykoudis (1978) study focussed on the near wake behind a porous disc and a sphere and they found distinct differences which they attributed to different vortex structures for the two cases. Some early studies (Calvert (1967*a*), Calvert (1967*b*)) showed that the large scale vortex shedding was more pronounced for an inclined disc than for a disc oriented normal to the flow. A typical Strouhal number (based on the diameter of the disc) when the disc is placed normal to the flow was 0.13 and this value increases (i.e. the shedding frequency increases) when the disc is inclined.

Only few wind tunnel experiments on the wake flow behind rotating wind turbine models have been made (see e.g. Alfredsson *et al.* (1982)) and they have mainly been limited to measurements of the streamwise velocity component in order to determine the wake development and the velocity deficit. Therefore it is of interest to also make measurements of the full velocity field (all three velocity components) behind the turbine. For instance Hansen & Butterfield (1993) points out that knowledge of all three velocity components in the flow field is essential in order to predict wind park rotor loads. It should also be noted that a full scale turbine works in the atmospheric boundary layer, i.e. in a turbulent environment and this will have an influence on the wake dispersion.

The connection between the wake behind a wind turbine rotor and that of a solid body is not altogether clear. The solidity, i.e. the ratio of the blade area to the swept area, is of the order of 5-15% (the lower value for a large scale turbine, the higher for a typical wind turbine model), but for increasing tip speed ratio the drag increases and therefore the blockage experienced by the flow goes towards that of a porous disc. The momentum deficit in the wake is directly coupled to the drag on the turbine and in this respect the turbine acts as an axis-symmetric body or disc. The torque on the turbine gives a similar torque back on the flow which will give the wake a slight rotation.

An interesting possibility to avoid or minimize the interaction between the wake and a downstream turbine is to actively yaw the upstream turbine (see Dahlberg & Medici (2003)). Since in that case the wind will also give a force on the turbine which is normal to the wind direction an equal force but in opposite direction will act on the wind, thereby deflecting the wake somewhat. In this paper we present results obtained with hot-wire anemometry showing the velocity distribution for all velocity components downstream the turbine both for flow normal to the turbine disc as well as for yawed conditions. For the latter case the wake deflection is clearly illustrated.

As mentioned, the rotating turbine gives rise to a flow blockage similar to that of a non rotating disc. Therefore it may also be anticipated that the regular large scale vortex shedding found behind solid discs should appear also for turbines. In this paper we describe wind tunnel experiments where such vortex shedding has been observed for the first time and we can show that this

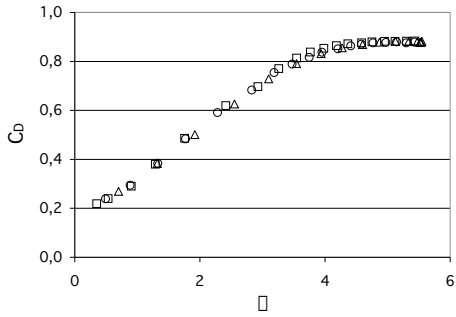

FIGURE 1. Drag coefficient as function of the tip speed ratio λ. ○: U_∞=8.3 m/s, no turbulence, □: U_∞=8.5 m/s, 4.5% grid turbulence, △: U_∞=5.5 m/s, no turbulence.

behaviour is close to what has been observed for solid discs. Finally it is hypothesized that this vortex shedding is the cause for the observed meandering of wakes measured behind full scale turbines.

2. Experimental set-up and methods

The experiment was performed in the MTL (Minimum Turbulence Level) wind tunnel at KTH Mechanics. The test section has a width and height of 1.2 and 0.8 m respectively, and its length is 7 m. The ceiling is adjustable, which makes it possible to provide a constant velocity in the streamwise direction despite the boundary layer growth on the test section walls. The maximum speed of the tunnel is more than 60 m/s, however for the present study a typical free stream velocity was 8 m/s. The wind tunnel provides stable conditions and the air temperature is controlled by means of a heat exchanger. Most of the measurements were made at low ambient turbulence level (less than 0.1%), however some measurements were made with a turbulence grid mounted 20 cm downstream the inlet. The grid is a monoplane grid, consisting of 10 mm square bars, with a mesh width of 50 mm. With the grid the turbulence level at the position of the turbine is about 4.5%.

The turbine model is two-bladed, with a diameter of 0.180 m and is mounted on the wind tunnel floor on the centreline, 1.45 m from the test section inlet. The height of the hub above the floor is 0.24 m. The non-twisted blade is based on the Göttingen 417A airfoil and has been built at FOI (Swedish Defense Research Agency), Stockholm. Details on the blades and their construction can be found in Montgomerie & Dahlberg (2003). The four-layered structure of reinforced epoxy composing the blade is about 0.5 mm thick. The maximum chord is 27 mm at 12% of the radius, and the tip chord is 16 mm.

In order to measure the drag on the turbine, the tower was mounted on a strain-gauge balance which is calibrated by applying a known force at the centre of the hub. In Fig. 1 the drag coefficient of the wind turbine model as

function of the tip speed ratio (tip speed/wind speed=λ) is shown. The data were measured both at 5 m/s and at 8 m/s, as well as with the turbulence grid mounted. The tip speed ratio was varied by keeping the wind speed constant, and changing the electrical loading of the generator from short circuiting to free-running (opened circuit) conditions. As can be seen the data for the different cases show a nice collapse. It can be noted how the drag coefficient tends to a value of 0.17, when linearly extrapolated to λ=0. This value seems reasonable if the blade can be be approximated with a flat plate with an aspect ratio of 4 (crudely resembling the blades used here). Such a plate has a drag coefficient of 1.17 (see e.g. Hoerner (1965)) and since the solidity of the turbine model is 13%, a value of 0.152 is obtained when applying the same percentage to the drag coefficient of a plate. This value is close to the extrapolated value of 0.17 at λ=0, so the behaviour of the wind turbine could be connected to that of a plate facing the flow when no rotational effects are present.

The velocity field was measured with two-component hot-wires (X-wires) which were calibrated against a Prandtl tube. The X-wires were built in the laboratory and had a measuring volume of 1 mm^3. One X-wire was fixed on the tip of a 2 m long sting, connected to the wind tunnel traversing system. It has 5 degrees of freedom: streamwise (x), vertical (y), spanwise (z), and the rotation of the probe around the x-axis and the y-axis. The latter degree of freedom, together with the computer-controlled movement, allowed an automatic calibration of the X-wires. Time-correlation measurements between two signals were also performed: a second X-wire was placed 1D downstream and on the right hand side of the turbine when looking from upstream, where the tip vortex had its centre. The X-wires acquired data at 5 kHz, for a typical sampling time of 30 sec. A photograph of the experimental set-up is shown in Fig. 2.

The coordinate system is centered in the middle of the rotor plane. Looking from upstream, the x-axis is directed in the undisturbed wind direction, the y-axis points upwards and the z-axis is positive towards the right hand side of the wind turbine model. The turbine is yawed around the centre of the rotor, but the coordinate system is kept fixed relative to the test section. A positive yaw angle is defined when the right hand side of the turbine is turned upstream.

3. Results

In the present experiments all three velocity components were measured at several downstream positions, ranging from x/D=0.5 to 9. The measuring grid in the cross-stream plane for the traversed probe was chosen to follow radial directions at 0° (corresponding to y=0 and varying the z-position on the positive side), and then anti-clockwise every 30° until 180° (y=0, negative z-positions). In each point the X-wire was turned around its x-axis so that either the streamwise and azimuthal velocity components or the streamwise and radial velocity components were measured. In this way the coupling between the azimuthal and the radial component was avoided. Along each radial direction measurements were taken at 18 positions, starting at the centreline (y=0, z=0

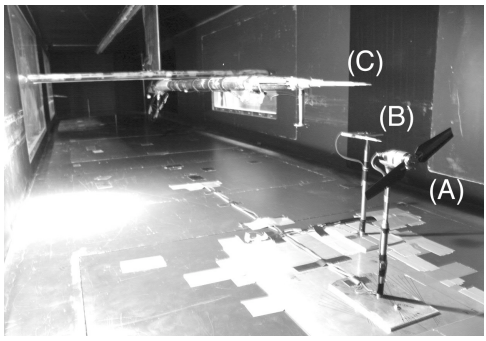

FIGURE 2. Experimental set-up. The view is from upstream looking downstream into the test section. The turbine model is marked with (A), the stationary X-wire used for the correlation (B) and the traversing system with the X-wire on the tip of the sting (C) are visible.

or r=0) and with the last position at r=330 mm. In the central part of the wake the step size is 15 mm, in the region of the tip vortices 7 points are taken with a step size of 4 mm, and in the outer region the step size increases to 20 mm. In the following only a few x-positions, which illustrate the flow development, are shown. The results are shown in mainly two different ways, I: vector plots of the cross stream velocity in the yz-plane, overlapped with contour-lines showing the streamwise velocity (see Fig. 3) and II: contour plots of each of the three components (see Fig. 4).

Fig. 3 shows the velocity field at x/D=1 as seen from the upstream side. The turbine is rotating clockwise, and the wake rotation is hence in the opposite direction. The free stream velocity is determined as the average result from the points $r/D \geqslant 1.4$ and is at this position determined to be 8.5 m/s. In the figure a reference velocity vector with a length corresponding to 1 m/s is also shown. The dashed contour lines represent lines of constant streamwise velocity. It is seen that the measured velocity field at this position has a fairly axis-symmetric appearance although some vectors in the plot, at a radius of approximately r/D=0.6, have a direction which is abruptly changing with respect to the surrounding vectors. This is probably because their positions correspond to the tip-vortex passage point.

The most apparent observation in Fig. 3 is the large values of the azimuthal velocity component. The largest azimuthal velocity is found around r/D=0.5 and is of the order of 1 m/s where the streamwise velocity is around 4 m/s. This would give a swirl flow angle of about 15° inside the wake.

To further illustrate the flow field in the wake we plot the three different velocity components separately, namely the streamwise, radial and azimuthal

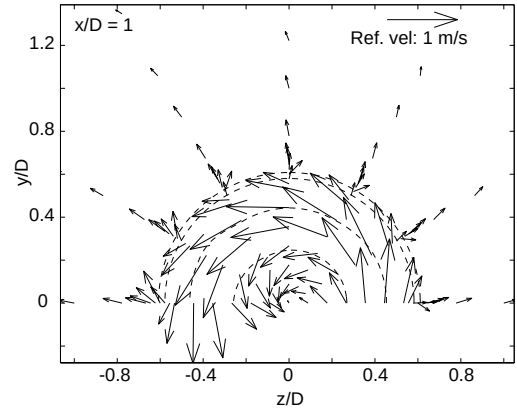

FIGURE 3. Velocity plots, no turbulence, no yaw, x/D=1, U_∞=8.5 m/s. The dashed contours are lines of constant streamwise velocity (2, 4, 6, 8 m/s).

components in terms of shaded contours. To construct this type of plot the values between the grid points are linearly interpolated at a constant radius for each component. The azimuthal component is considered positive if clockwise, i.e. in the same direction as that of the turbine rotation and all the velocity components are normalized with the free-stream value.

Fig. 4 shows the corresponding contour plots. In this representation it is clear that the flow field shows a high degree of axis-symmetry, although some differences are seen especially in the radial component. The reason could be a non-perfectly symmetric positioning of the hot-wire probe with respect to the real wake centre. The radial velocity shows that the flow field is expanding both in the outer part of the wake as well as outside the wake, but in the core region the radial velocity is directed towards the centre. The change in sign appears for this case at approximately r/D=0.38. Inspection of other cross stream planes shows that already at x/D=1.5 the radial velocity is negative everywhere, indicating that the entrainment of fluid into the wake also affects the flow outside the wake itself.

3.1. *Wake under yawed conditions*

In order to fully utilize the potential of using yaw as an active control on the wind turbine (see Dahlberg & Medici (2003)) it is necessary to have a good knowledge of the velocity field downstream the yawed turbine, especially with respect to the horizontal velocity component normal to the wind direction and the resulting wake displacement. Some velocity measurements, mainly of the streamwise velocity, downstream of a yawed turbine has earlier been

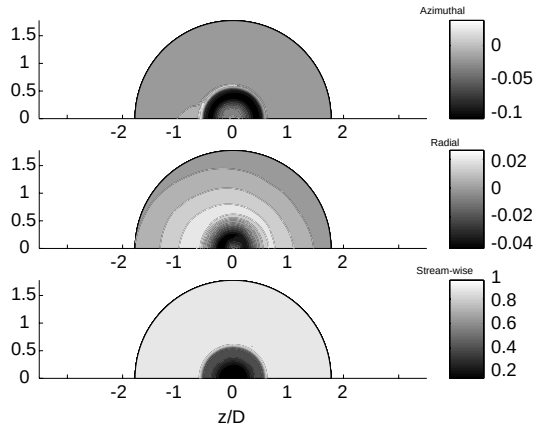

FIGURE 4. Same data as in Fig. 3, but the components are separated. The three figures show from top the azimuthal, radial and streamwise velocity components, respectively. All velocity components are normalized with the free stream velocity.

carried out using PIV (see Parkin *et al.* (2001)). In the present study we have determined the three-dimensional velocity field downstream a yawed turbine, using hot-wires, to better understand the phenomena involved. Measurements were made for yaw angles (γ) 0°, 10° and 20° although only the results for 0° and 20° are shown in this paper.

Fig. 5 shows the vector plots with γ=20° at x/D=4. The wake is no longer axis-symmetric and the displacement and deformation of the streamwise contour lines toward the left hand side is clearly visible, as a response to the side force on the turbine in the positive z-direction.

The contour plots in Figs. 6 and 7 show the change of the displacement of the wake under yawed conditions ($\gamma = 20°$) at x/D=4 and 9. This is most evident from the streamwise velocity component where the wake minimum is shifted approximately $0.5D$ towards negative z at x/D=4 and even further to the left downstream. Also the radial component is towards negative z, although its magnitude is reduced by a factor of two between the two positions.

3.2. *Free-stream turbulence*

In the present study we have also investigated the influence of free stream turbulence of the near wake. A passive grid was used to create free-stream turbulence. The value of the turbulence intensity was 4.5% of the free-stream velocity at the turbine position and has decayed to 2.5% at x/D=9. It is well known that the wake will recover faster when influenced by free stream

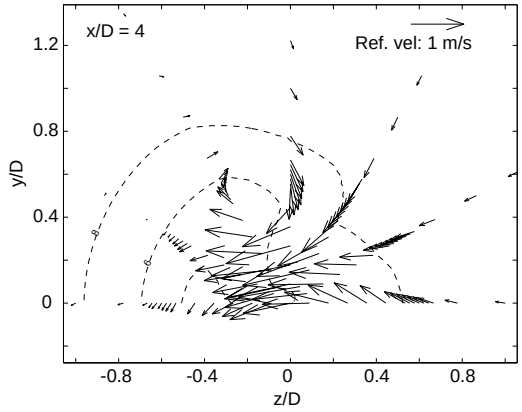

FIGURE 5. Vector plot for $\gamma = 20°$, $x/D = 4$. Positive yaw is for the right hand side of the turbine moved upstream.

turbulence, however the behaviour of the wake immediately downstream the rotor plane is not well studied. The same measurements as for the case with no turbulence, were made and in Fig. 8 the streamwise velocity for the two cases are compared. It is clearly seen that the initial wake is quite similar in the two cases up to x/D=2 but the influence of the free stream turbulence is clearly seen at x/D=3. It can also be noted that the drag coefficient is similar for the two cases (see Table 1). The small difference may be explained by the fact that the loading circuit only allows finite control steps. This also indicates that the momentum defect in the wake should be the same. Also if the two other velocity components are compared for the two cases the differences are negligible close to the turbine.

	λ	C_D
No turbulence grid	3.66	0.816
4.5% FST	3.73	0.835

TABLE 1. Drag coefficient of the turbine with and without free-stream turbulence (FST).

3.3. *Bluff-body vortex shedding*

The flow that approaches the turbine rotor feels the turbine as an object giving a drag force, much the same way as a bluff body or disc would. A characteristic of bluff body flows is the so called vortex shedding, maybe most known as the

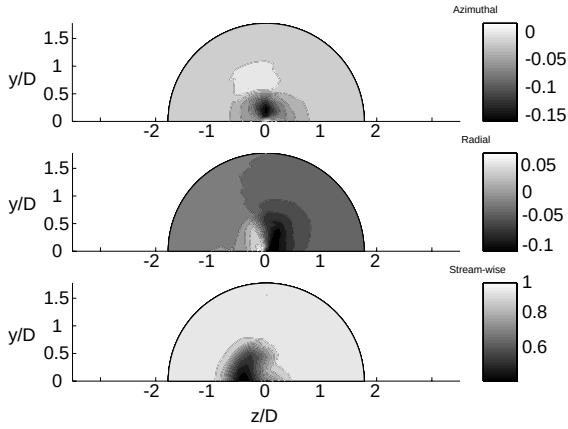

FIGURE 6. Same data as in Fig. 5, $\gamma = 20°$ and $x/D = 4$.

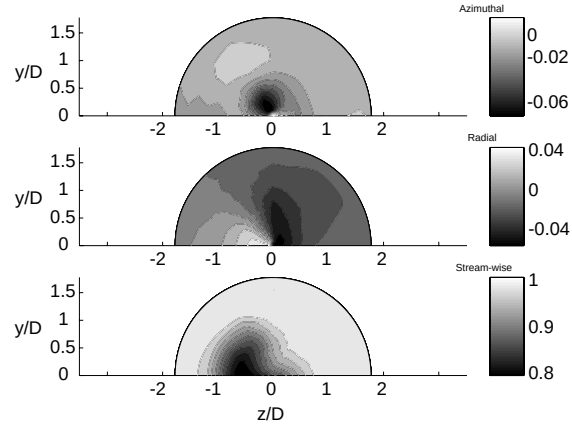

FIGURE 7. Same conditions as Fig. 6. $x/D = 9$.

Karman vortex street for two-dimensional cylinders. However vortex shedding may also appear behind three dimensional bluff bodies such as circular discs.

When the time signal of the streamwise velocity was observed in the region of the tip-vortices a very strange behaviour was detected. The signal shown in Fig. 9 is an example of such a signal. The signal shows velocity peaks which can be identified as peaks coming from the tip vortices themselves with a time interval of about 10 ms, corresponding to one vortex shed by each blade per revolution giving twice the rotation frequency (approximately 55 Hz) of the turbine. However this signal seems to be overlayed by a much lower frequency

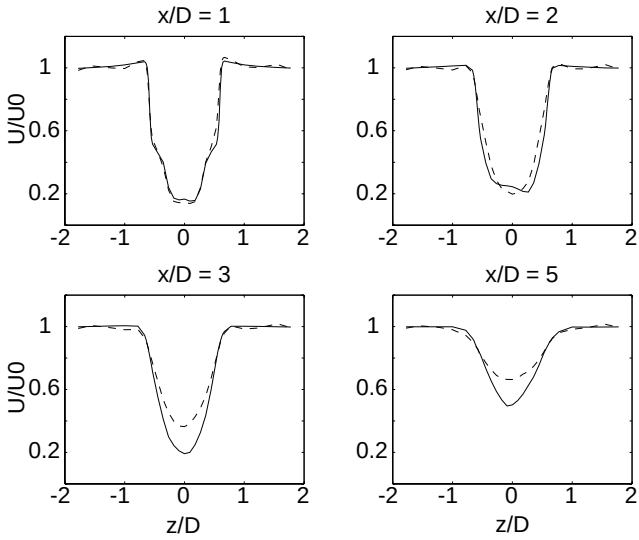

FIGURE 8. Difference between the streamwise velocity without free-stream turbulence (solid line) and with turbulence (dashed line). x/D=1, 2, 3, 5.

than that of the tip vortices themselves. Also the signal of the radial component (Fig. 10) shows a modulation with the same low frequency. If a frequency analysis of the time signals is made, a clear peak in the energy spectrum at 7.9 Hz is seen. This frequency is not only detected in the wake but also in the free-stream and for all three velocity components. Our hypothesis is that this behaviour is connected with vortex shedding from the turbine disc, much in the same way as one would expect for a solid disc. This may also be connected to the observed "meandering" of wakes downstream of full scale turbines. In the following we will show that the data may be interpreted in this way.

In a coordinate system following the centre of the tip vortex, the vortices may be viewed as a central core rotating as a solid body and an outer rotating flow with a decreasing rotational velocity with increasing r. With respect to the reference frame of the laboratory, the centre of the tip vortex may be viewed as convected with a velocity which is close to the mean velocity of the flow at that position. If the radial position of the measuring point is at the outer part of the tip-vortex with respect to the wake centre, the measurements of the streamwise velocity will show a high velocity peak at every vortex passage. On the other hand, if the measurement point is in the inner part of the vortex, the velocity signal will show a periodic velocity dip.

A time signal with the appearance shown in Fig. 9 can on the other hand be obtained if the probe is very close to the centre of the vortex, and the wake

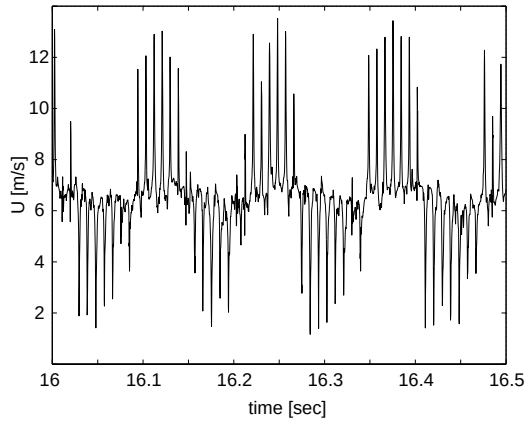

FIGURE 9. Time signal of the streamwise velocity close to the centre of the tip vortices (x/D=1, y/D=0, and z/D=0.6), clearly showing the 7.9 Hz fluctuation.

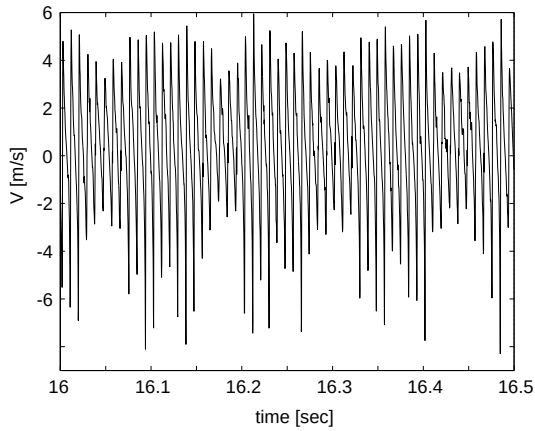

FIGURE 10. The radial velocity component at the same position and time as in Fig. 9.

and hence the tip vortices are moving radially at a low frequency in such a way that the two sides of the vortex are alternating at the probe position. It can also be noted that the amplitude of the radial velocity signal varies in relation to the downstream velocity: when the streamwise velocity has an overshoot, the amplitude of the radial component is larger, whereas when the inner side of the vortex is passing the measuring point, a lower amplitude of the radial velocity can be observed. The reason for this may be due to the fact that the probe is not located exactly at the centre of the tip vortex.

Short time segments taken from Figs. 9 and 10 are shown in Fig. 11. It

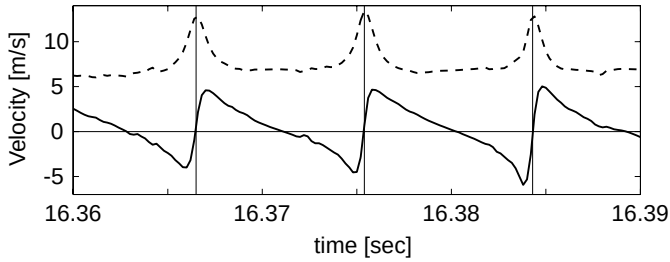

FIGURE 11. Close-up on the streamwise component (dashed) and radial component (solid line) of the velocity. Three vertical lines passing through the peaks of the streamwise velocity are plotted as reference, together with the zero velocity axis.

is clearly seen that the maximum in u is where v=0, which is what would be expected during a vortex passage. The v-signal is also shown to be antisymmetric with respect to its zero passage and finally we can observe that the largest (absolute) value of v is about the same as the velocity increase between the base level of u and that of the measured peak. All these results are in accordance with the idea of the tip vortex passage.

The close up of the time signal in Fig. 11 shows how the probe is at first measuring the approaching of the vortex by the radial velocity becoming negative, then in correspondence of the vortex core (i.e. between the negative and the positive peaks of the velocity) the peak in the streamwise velocity is observed. If the time between the peaks of the streamwise velocity equals the shedding frequency, the time between two peaks of opposite sign of the radial velocity can give information about the vortex core radius. An exact value of this time can not be given, since as discussed above the position of the probe is not exactly symmetric with respect to the vortex centre and therefore the measured time changes. An estimate gives a value of the order of 1 ms. Correlation measurements which are reported in section 3.4 show that the propagation speed of the vortices at this position is about 6.4 m/s, which is lower than the free stream velocity (8.3 m/s) but similar to the local streamwise velocity in between the peaks representing the vortices in Fig. 11. This means that the diameter of the vortex core is around 6–7 mm.

As mentioned above, another important result which can be noted from the time signals is a low frequency shedding. This phenomenon is detected in all the velocity components, indicating that the shedding is three-dimensional. The shedding frequency f can be normalised using the diameter of the turbine D and the local free-stream velocity, as it is usually done for bluff bodies. The

resulting non-dimensional frequency, the so called Strouhal number, is then defined as:

$$St = \frac{fD}{U_\infty}$$

For a bluff body like a disc, St is independent of the Reynolds number if the Reynolds number is sufficiently high.

The frequency of the bluff body shedding was obtained through spectral analysis (FFT) from the time signals of the streamwise velocity measured at x/D=1 and in the region where the tip vortices are found. The Strouhal number as function of the tip speed ratio can be found in Fig. 12. The data shown are for U_∞=8.5 m/s and 8.3 m/s with and without free stream turbulence, as well as measurements at U_∞=5.5 m/s without FST. First of all it can be noted that no data points were obtained for cases with λ smaller than 3. A plausible explanation is that for lower λ than 3 the flow does not see the blockage as a disc, but rather sees the individual passage of the blades which thereby does not give rise to the large scale vortex shedding. As can be seen, the Strouhal number decreases with increasing tip speed ratio and for λ>4.5 it levels out around 0.12. This value is similar to what has been reported for solid discs. It is interesting to note that the drag coefficient also is nearly constant for λ>4.5 (see Fig. 1). The increase in St for smaller λ may be seen as a decrease of the effective

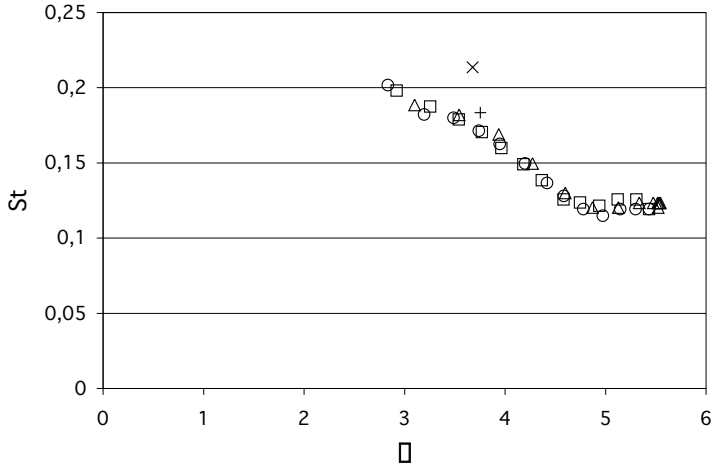

FIGURE 12. Strouhal number as function of the tip speed ratio λ with yaw angle γ=0. ○: U_∞=8.3 m/s, no turbulence, □: U_∞=8.5 m/s, 4.5% grid turbulence, △: U_∞=5.5 m/s, no turbulence. Also two data points with γ=10° (+) and γ=20° (×) are included.

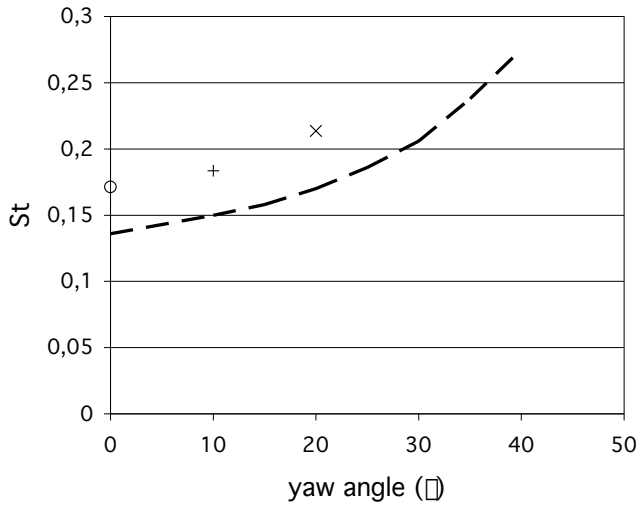

FIGURE 13. Strouhal number as function of the yaw angle, compared with the behaviour of a disc (from Calvert (1967*a*)). Same data as in Fig. 12, with the data point for γ=0 taken at λ=3.74.

diameter of the turbine with respect to the vortex shedding phenomenon. A similar result is seen for the turbine under yawed conditions; the St is larger than for the zero yaw case, suggesting a smaller effective diameter of the yawed turbine.

The results for the yawed turbine could also be compared with the results of a yawed disc reported by Calvert (1967*a*). The same data as in Fig. 12 ($\lambda\approx$3.7) are plotted in Fig. 13 and the change of St is seen to be similar as compared to the data from the disc, although the absolut values are shifted somewhat.

3.4. *Space-time structure of the wake*

In order to obtain further understanding of the space-time structure of the vortex shedding behind the turbine we carried out measurements using two X-probes which were separated in space. One probe (named probe 2) was stationary and placed at x/D=1, y/D=0 and z/D=0.6. The other probe (probe 1) was mounted on the traversing system and could hence be moved with respect to the stationary probe. For the measurements presented in the following this probe was located on the other side of the turbine (i.e. negative z) at y/D=0, and moved both in the spanwise direction (111 points starting at z=–80 to –300 mm with a step length of 2 mm) and at different x.

In order to illustrate the correlation between the two signals, Fig. 14 shows

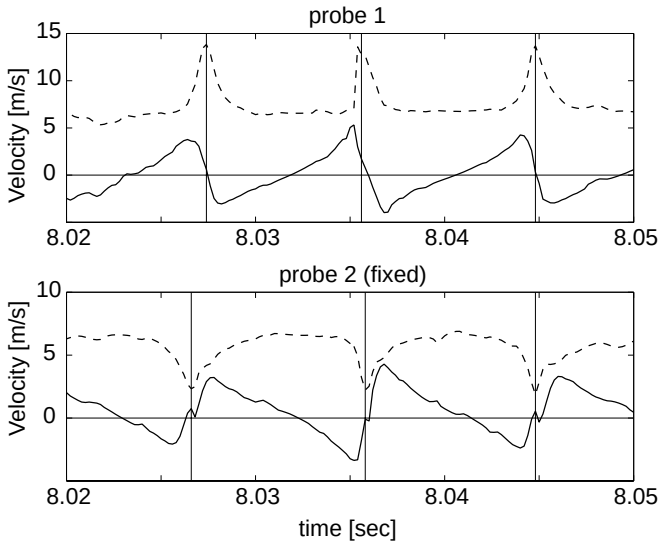

FIGURE 14. Velocity traces for two probes at x/D=1 and y/D=0, with z = –104 mm (probe 1, top) and z = +108 mm (probe 2, bottom). The dashed lines correspond to the streamwise velocity and the full lines to the velocity in the z-direction.

the velocity signals obtained from the X-wires when they are placed in opposite positions with respect to the wake centreline, at the same downstream position. The velocity signals corresponding to the spanwise velocity show the expected behaviour, the velocity measured by probe 2 is a mirror image of the signal from probe 1. On the other hand the streamwise velocity signals show a behaviour which indicates that probe 2 is on the inner side of the vortex whereas probe 1 is on the outer side. Now the picture for the streamwise velocity may change due to the meandering of the wake as was seen in Fig. 9, whereas the spanwise signal will qualitatively stay the same. Note that probe 2 in Fig. 14 is at the same position as for the measurements shown in Fig. 11, however the time sequence here is for the case when the vortices have shifted outwards with respect to the probe, giving a decrease in the streamwise velocity during the vortex passage.

The space-time structure of the wake can be further elucidated by calculating the correlation between the velocity signals at the two positions. The correlation $R_{u_1u_2}(\tau)$ between the signals $u_1(t)$ and $u_2(t)$ (both with zero mean) is defined as

$$R_{u_1u_2}(\Delta t) = \frac{1}{u_{1rms}u_{2rms}} \frac{1}{T} \int_{-T/2}^{T/2} u_1(t+\Delta t)u_2(t)dt \qquad (1)$$

where u_{1rms} and u_{2rms} are the rms values of the two signals. The time delay Δt can then be used to show how a disturbance propagates in the flow field. As

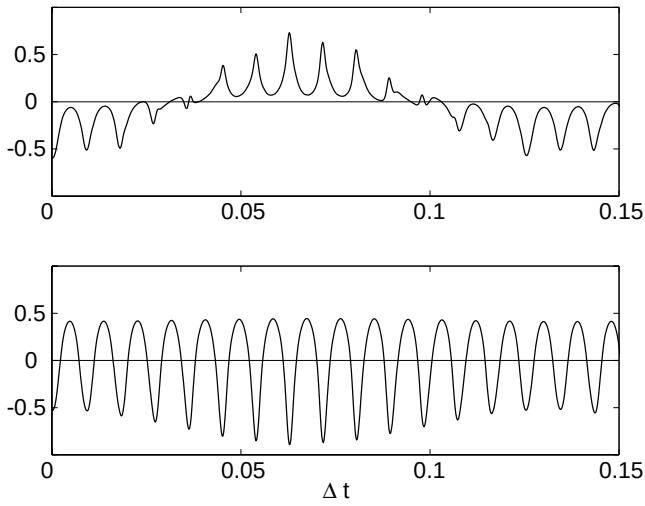

FIGURE 15. Correlation coefficients between the streamwise velocities (top) and the spanwise velocities (bottom) as function of the time displacement between the signals.

an example the correlation between the signals in Fig. 14 are shown in Fig. 15. The figure shows both the frequency of the tip vortices themselves as well as the frequency connected to the large scale shedding.

The time correlation was computed for each of the 111 measurement points in the spanwise direction, between $z/D = -0.44$ to $z/D = -1.67$. The results can be seen in Figs. 16–18. In these figures the time axis has been made non-dimensional with the free stream velocity and the rotor diameter. Both the correlation between the streamwise velocity components and that between the spanwise components are shown. In Fig. 16 both probes are placed at x/D=1. In the spanwise component the tip vortices are clearly observed for the whole displayed time interval which shows that the frequency and signals are very steady. The vortices are also seen in the correlation of the streamwise velocity, however it is less clear so. The main difference between the plots are found in the outer region, where a periodicity of much larger time scale is found in the streamwise correlation. The correlation time length is the same as that of the large scale shedding from the turbine. It is interesting to note that it can be clearly detected far outside the wake region. Similar results are observed also at x/D=2 in Fig. 17, although the correlation is overall smaller and for the streamwise velocity it becomes more blurred in the region of the tip vortices, whereas at x/D=3 (see Fig. 18) the correlation for the streamwise component of the tip vortices has vanished. It is however still quite clear in the correlation for the spanwise component. At this position it can be noted that the large scale shedding is dominating for the streamwise component and this picture is seen even further downstream (not shown here). This indicates that the large

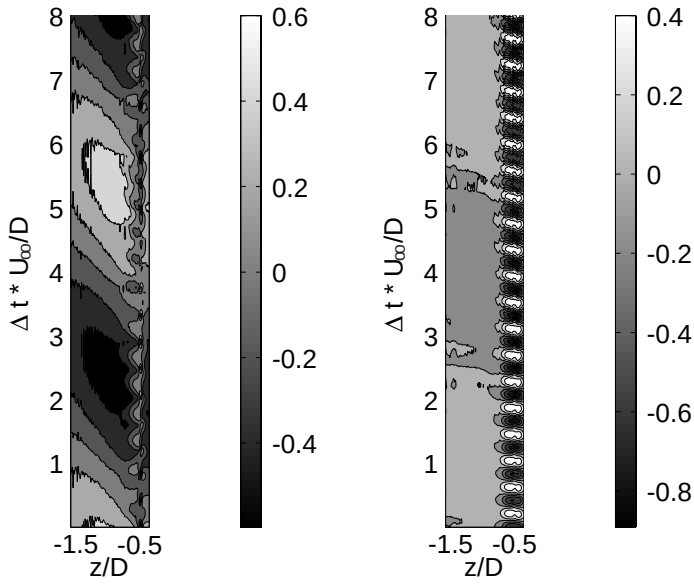

FIGURE 16. Correlation between velocities measured measured with both probes at x/D=1. The fixed probe is at z=108 mm, i.e. x/D=0.6. Left: correlation between the streamwise velocities. Right: correlation between the spanwise velocities.

scale shedding is persistent and may influence the motion in the wake region.

As was mentioned previously in section 3.3 the correlation results in the tip vortex region shown here were used to calculate a propagation speed of the tip vortices, by following for instance one maximum in the downstream direction. In this way the propagation speed of the tip speed vortices was found to be about 75% of the free stream velocity.

4. Conclusions

The present work has focussed on the development of the near wake region behind a wind turbine model. For the first time the full velocity field, i.e. all three velocity components, has been measured, showing among other things quantitative data on the wake rotation. Also the influence of yawing the turbine on the deflection of the wake has been shown.

The most interesting finding was however the low frequency shedding from the turbine. The frequency of this shedding is an order of magnitude smaller than that of the blade frequency and the phenomenon seems to be similar to the vortex shedding occurring for solid discs. Previously the meandering of turbine wakes which has been observed in field measurements, has been interpreted as

a result of the transverse velocity fluctuations of the wind (see e.g. Thomsen *et al.* (2001)), however the observed shedding may be a more likely candidate responsible for the meandering motion.

Acknowledgements

The work was sponsored by the Swedish National Energy Agency (STEM). The authors thank Jan-Åke Dahlberg (FOI) for providing the model and for many fruitful discussions.

References

Alfredsson, P. H., Dahlberg, J. Å. & Vermeulen, P. E. J. 1982 A comparison between predicted and measured data from wind turbine wakes. *Wind Engng.* **6**, 149–155.

Bevilaqua, P. M. & Lykoudis, P. S. 1978 Turbulence memory in self-preserving wakes. *J. Fluid Mech.* **89**, 589–606.

Calvert, J. R. 1967*a* Experiments on the flow past an inclined disk. *J. Fluid Mech.* **29**, 691–703.

Calvert, J. R. 1967*b* Experiments on the low-speed flow past cones. *J. Fluid Mech.* **27**, 273–289.

Dahlberg, J. Å. & Medici, D. 2003 Potential improvement of wind turbine array efficiency by active wake control (AWC). In *Proc. European Wind Energy Conference and Exhibition*, Madrid, (published on CD).

Hansen, A. C. & Butterfield, C. P. 1993 Aerodynamics of horizontal-axis wind turbines. *Annu. Rev. Fluid Mech.* **25**, 115–149.

Hoerner, S. F. 1965 *Fluid-dynamic drag*. Hoerner Fluid Dynamics.

Johansson, P. B. V., George, W. & Gourlay, M. J. 2003 Equilibrium similarity, effects of initial conditions and local Reynolds number on the axisymmetric wake. *Phys. Fluids* **15**, 603–617.

Montgomerie, B. & Dahlberg, J. Å. 2003 Vortex system studies on small wind turbines. FOI scientific report, ISRN FOI-R–0936–SE.

Parkin, P., Holm, R. & Medici, D. 2001 The application of piv to the wake of a wind turbine in yaw. In *Proc. 4th International Symposium on Particle Image Velocimetry*, PIV'01, Göttingen (Ed. J. Kompenhans) DLR-Mitteilung 2001–03 (published on CD).

Thomsen, K., Madsen, H. A. & Larsen, G. C. 2001 A new method can predict detailed response for turbines in wind farms. In *Proc. IEA 16th Symp. Aerodyn. Wind Turbines*, Boulder, FOI–S–0877–SE, pp. 171–187.

Vermeer, L. J., Sørensen, J. N. & Crespo, A. 2003 Wind turbine wake aerodynamics. *Prog. Aerospace Sci.* **39**, 467–510.

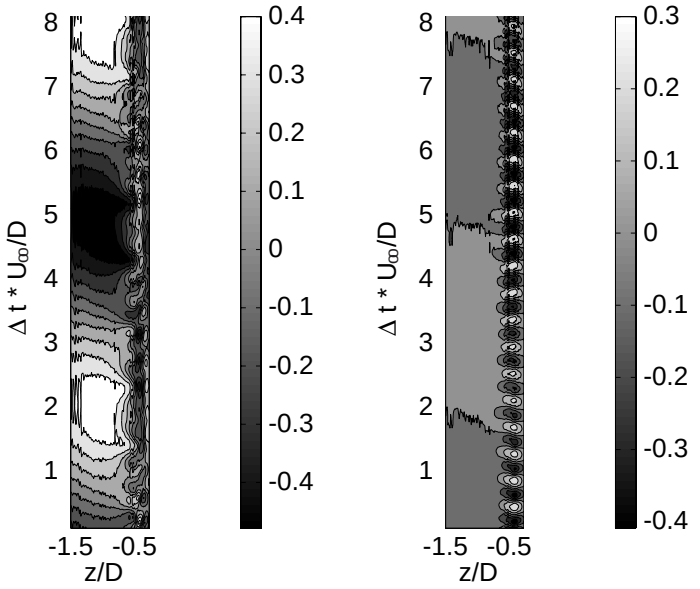

FIGURE 17. Same type of data as in Fig. 16, but with the movable probe at x/D=2.

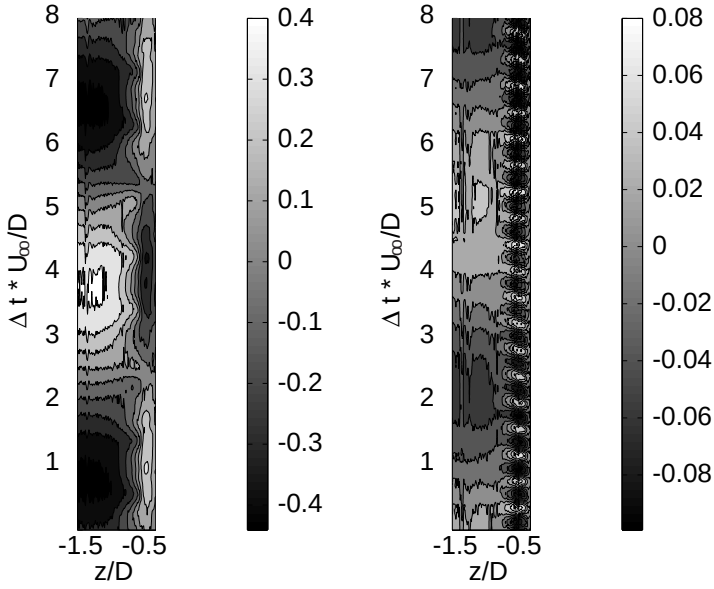

FIGURE 18. Same type of data as in Fig. 16, but with the movable probe at x/D=3.